Trends in man-made and natural cirrus clouds for the period 1984-2004

Kostas Eleftheratos*, Christos S. Zerefos
Laboratory of Climatology & Atmospheric Environment, University of Athens, Greece

Patrick Minnis
NASA Langley Research Center, Hampton VA, USA

Keywords: Cirrus clouds, trends

ABSTRACT: This study compares trends in man-made and natural cirrus clouds with aviation flown distance and with trends in natural parameters over the tropical and middle latitudes i.e., over regions dominated by dynamics in comparison with regions where microphysics explains most of the variance in cirrus cloud cover. Results presented in this study generally confirm earlier findings on possible effects of aviation on cirrus cloud positive trends over congested air traffic regions. More specifically, the longitudinal distribution of cirrus cloud trends from 1984 to 2004 is positively correlated (+0.6) with the spatial distribution of aviation flown distance over the northern middle latitudes and not over the tropics. In the tropics it is shown that cirrus cloud trends are correlated with trends in vertical velocities and with trends in relative humidity.

1 INTRODUCTION

Aircraft flying at high altitudes may form contrails. Contrails are line shaped clouds forming behind an aircraft if the ambient air is cold enough (Schumann, 1996). In dry air the contrails dissipate quickly, and their impact is of minor importance, but in moist air which is super-saturated with respect to ice, the contrails spread and grow with the uptake of ambient water vapour, and become contrail-cirrus (Schumann, 2005). Contrail-cirrus would not exist without the prior formation of contrails (i.e., Gierens, 2006). Figure 1 shows some examples of linear persistent contrails and contrail-cirrus in the atmosphere based on observations from ground. This kind of cirrus formation occurs in regions with high air traffic (i.e., North America, North Atlantic, Europe).

Recent studies (i.e., Minnis et al., 2001; Zerefos et al., 2003; Minnis et al., 2004; Stubenrauch and Schumann, 2005; Stordal et al., 2005; Mannstein and Schumann, 2005; Krebs, 2006) have examined the possible influence of air traffic emissions on cirrus cloud positive trends using various methods and different datasets for different periods of records. Major findings of those studies were summarized in Gierens (2006). For example, in central Europe it was found that the observed positive trends in cirrus due to aircraft are about 1-2% cover per decade. Mannstein and Schumann (2005) had estimated ~3% additional cloud coverage due to aircraft over Europe, which is about ten times higher than the coverage by linear contrails (~0.3%) alone. However, their conclusion that the coverage by additional cirrus clouds in Europe is about 10 times higher than by linear contrails is no longer supported (Mannstein and Schumann, 2007).

As air traffic increases (~5% per year), manmade (aviation) cirrus clouds are expected to increase. These additional clouds contribute to the greenhouse effect (i.e., Minnis et al., 2004; Sausen et al., 2005). However, present knowledge of the coverage and radiative forcing of manmade cirrus clouds is still poor. This kind of cirrus cloud might responsible for up to a doubling of the present estimate of aviation radiative forcing. If this is true, then the contribution of aviation to the total anthropogenic radiative forcing (which is ~3.5% for 1992 aircraft operations) might be doubled.

* *Corresponding author:* Kostas Eleftheratos, Laboratory of Climatology & Atmospheric Environment, Faculty of Geology & Geoenvironment, University of Athens, 15784 Athens, Greece. Email: kelef@geol.uoa.gr

Figure 1. Examples of linear persistent contrails and contrail-cirrus in the atmosphere.

This study compares changes in contrail-cirrus and natural cirrus clouds with aviation travelled distance and with changes in natural parameters. Correlations are sought over the tropical and middle latitudes i.e., over regions dominated by dynamics in comparison with regions where microphysics explains most of the variance in cirrus cloud cover. The main purpose is to relate and to attribute long-term changes in cirrus cloud cover to natural and anthropogenic (aviation-related) sources. The natural parameters used in this study are vertical velocities and relative humidity at 300 hPa. The level of 300 hPa was considered in this study as a standard level for highflying air traffic in the northern middle latitudes.

2 DATA SOURCES

The cloud data set analysed in this study was produced by the International Satellite Cloud Climatology Project (Rossow and Schiffer, 1999). The data are based on observations from a suite of operational geostationary and polar orbiting satellites. Visible radiances are used to retrieve the optical thickness of clouds and infrared radiances to retrieve cloud top temperature and pressure. The D2 dataset used in this study has a spatial resolution of 280 km (2.5^{o} at the equator) and provides monthly averages of cloud properties of fifteen different cloud types. The cloud types are derived based on radiometric definitions that rely on cloud optical thickness and cloud top pressure. Cirrus clouds are defined as those with optical thickness less than 3.6 and cloud top pressure less than 440 hPa. In this study we made use of the cirrus cloud data for the period 1984-2004.

The ISCCP cloud properties have been tested extensively both against other satellite cloud retrievals and against surface cloud observations (Rossow and Schiffer, 1999). In the latest (D-series) version of the ISCCP dataset, changes in the retrieval thresholds and the inclusion of an ice microphysics model for retrieval of optical thicknesses and top temperatures of cold clouds, have improved the agreement of cirrus cloud amounts with both surface observations (Rossow and Schiffer,

1999) and High-Resolution Infrared Sounder (HIRS) data (Stubenrauch et al., 1999). An underestimate of ISCCP cirrus clouds amounts (~5% at northern middle latitudes) compared to HIRS results is caused by missed detection of very thin clouds (Stubenrauch et al., 1999; Rossow and Schiffer, 1999). Moreover, high cloud amounts from this data set have been compared with those from SAGE II (Liao et al., 1995). It has been shown that the frequency of high-level clouds from SAGE II is about 3 times higher than the cloud amount from ISCCP with little seasonal variation. Despite this large systematic difference it was noted that the correlation between the zonal mean curves is high, 0.88 (99.99% confidence level) for July and 0.82 (99.99% confidence level) for January, which strengthens our results.

Vertical velocities and relative humidity at 300 hPa were analysed using the NCEP Reanalysis datasets for the period 1984-2004. NCEP provides mean monthly gridded values of various atmospheric and surface parameters on 2.5^{o}x2.5^{o} grid boxes and on global scale. We made use of the monthly daily means which are monthly means from base times 0000, 0600, 1200 and 1800 UTC (http://www.cdc.noaa.gov/data/gridded/data.ncep.reanalysis.html).

To overcome the effect of seasonal variations in the estimated trends, all trends were calculated after removing variations related to the seasonal cycle of the data. Cirrus cloud data were deseasonalized by subtracting the long-term monthly mean (1984-2004) pertaining to the same calendar month. All trends were evaluated as to their statistical significance by applying the t-test of each trend against the null hypothesis of no-trend for the appropriate number of degrees of freedom. CCC data for the years 1991 and 1992 were not used in our analysis in order to minimize artificial satellite cloud retrievals after the eruption of Mt. Pinatubo in 1991 (Rossow and Schiffer 1999; Luo et al., 2002).

3 RESULTS AND DISCUSSION

Figure 2 shows the spatial distribution of aviation travelled distance at 9760–11590 m height in the wintertime (January, February and March) (in km). Regions with heavy air traffic (more than 40.000 travelled km) are shown by dark grey and black colours while regions with lower air traffic (less than 40.000 km) are shown by light grey colours. In the northern middles latitudes (35^{o}-55^{o}N), congested air traffic regions are found over the US, Europe, and Japan, and over the North Atlantic and North Pacific Oceans. In the tropics (5^{o}-25^{o}N), regions with high air traffic are mainly observed over the Southeast Asia air traffic corridors and over the Caribbean Sea.

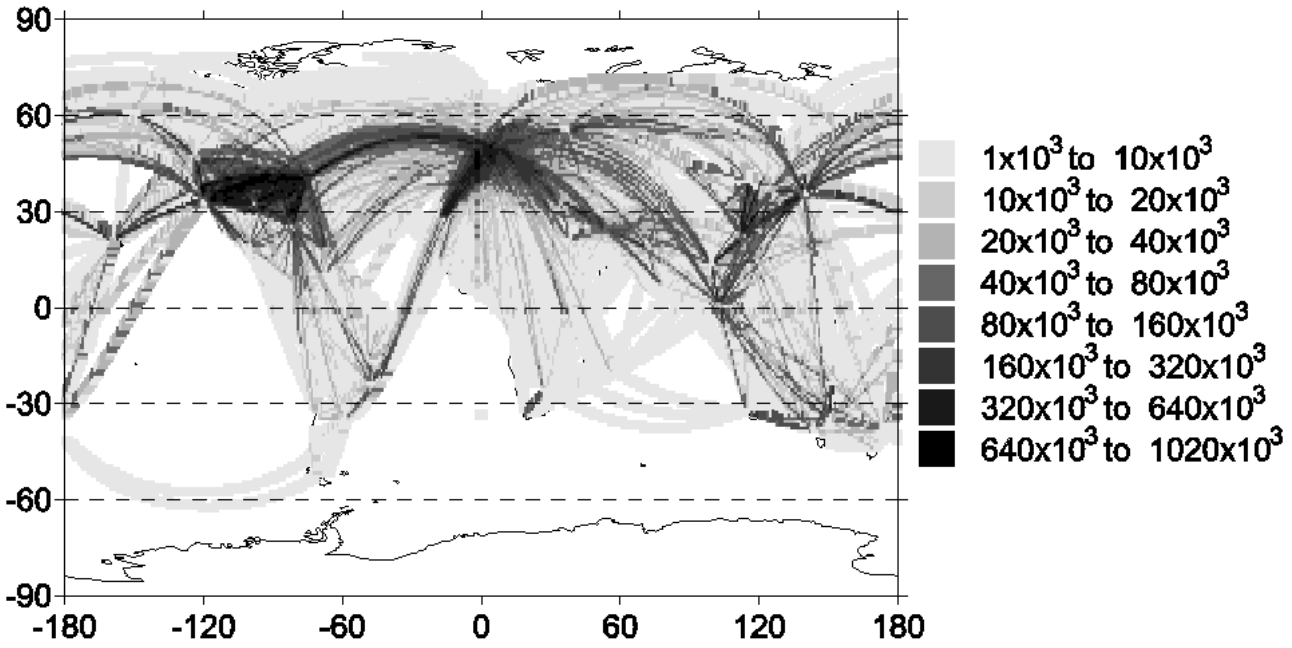

Figure 2. Travelled distance by aviation at 9760–11590 m height in 2000 in the wintertime (January, February and March) (in km/month).

In order to investigate whether cirrus cloud trends are correlated with air traffic, aiming at quantifying changes in cirrus cloudiness due to contrail formation by aviation, we have spatially correlated the cirrus cloud trends with travelled distance by aviation over areas that correspond to different air traffic load: (a) over the high air traffic northern middle latitudes (35^o-55^oN) and (b) over low air traffic tropical regions between (5^o-25^oN). Cirrus cloud trends could also be related to dynamical and thermo-dynamical variability. As a tracer of dynamics (convective activity) in the upper troposphere we made use of the monthly vertical velocities at 300 hPa (VV300). As a tracer of thermo-dynamical variability over the studied areas we analysed trends in relative humidity at 300 hPa (RH300). Figure 3 (upper panel) shows the longitudinal distributions of cirrus cloud trends from 1984 to 2004 and of aviation travelled distance in 2000 for the cold period (January, February and March).

As can be seen from Fig. 3a the longitudinal distribution of CCC trends over the northern middle latitudes is well correlated with travelled distance by highflying air traffic (correlation coefficient, R= +0.6), which agrees with the results presented by Zerefos et al. (2003). The positive correlation between the two variables suggests that the apparent increase of thin cirrus coverage, about 1.4% over North America and 0.5% over Europe, could be possibly related to contrail formation by aviation. Over East Asia on the other hand, there are negative trends in CCC which are related to negative trends seen in relative humidity (Zerefos et al., 2007). Negative trends over East Asia were also found by Minnis et al. (2004) who analysed cirrus/high clouds from ground-based data. For the summertime we note that the largest increases in CCC are found over the North Atlantic flight corridor (~2.1% per decade) (not shown here).

At lower latitudes (5^o-25^oN), where air traffic density is lower, the correlation between cirrus trends and aviation is insignificant (Fig. 3b). However the longitudinal variability of CCC is as high as that over the middle latitudes. This is not a paradox and can be explained by the fact that in tropical latitudes, cirrus clouds are formed primarily from vertical water vapour transport by convective processes (Zerefos et al., 2003). As a result, tropical cirrus amounts are controlled by local temperature conditions and moisture sources and any trend in those conditions would leave a signature on the cirrus cloud field. Therefore, the tropical cirrus trends could reflect trends in the local temperature and moisture field. In the middle latitudes, on the other hand, cirrus cloud formation is largely controlled by baroclinic processes that are to a great extent independent of local conditions and depend on global wave patterns. Therefore, any localized modulation of middle latitude cirrus cloud properties would be related more strongly to microphysical rather than dynamical condition changes (Zerefos et al., 2003). The results are shown in Figs. 3c, 3d, and in Figs. 3e, 3f where it appears that the observed trends in cirrus clouds are significantly correlated with corresponding trends in VV300 and RH300 over the tropics (–0.4 and +0.8, respectively) but not over the middle latitudes.

Our findings on the positive trends in cirrus clouds over the US, North Atlantic and Europe due to air traffic are consistent with those published by Zerefos et al. (2003), Minnis et al. (2004), Stordal et al. (2005), Stubenrauch and Schumann (2005) and Eleftheratos et al. (2007) even though there are considerable differences among the examined datasets and periods of records.

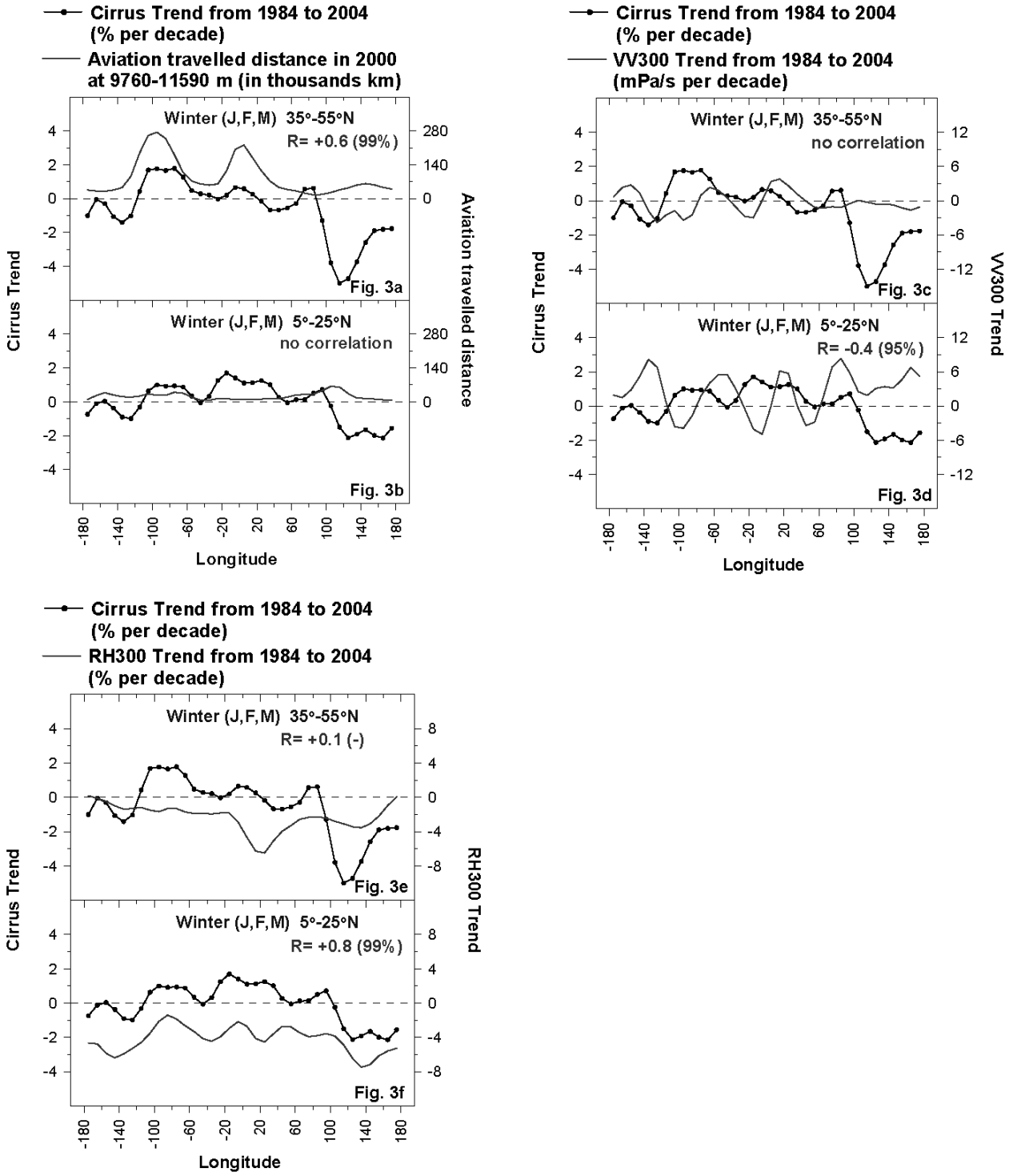

Figure 3. (Upper left panel) Longitudinal distribution of cirrus trends from 1984 to 2004 in the wintertime (Jan, Feb, Mar) versus the spatial distribution of aviation travelled distance in 2000 over: (a) heavy air traffic regions (35°-55°N), and (b) over low air traffic regions (5°-25°N). (Upper right panel) Same as in upper left panel but for cirrus trends and VV300 trends, respectively. (Lower left panel) Same as in upper left panel but for cirrus trends and RH300 trends, respectively.

4 CONCLUSIONS

Long-term changes in cirrus cloud cover from ISCCP satellite data have been correlated with aviation flown distance and compared with changes in natural parameters (vertical velocities and relative humidity at 300 hPa) over the middle and tropical latitudes. Results presented in this study generally confirmed earlier findings on possible effects of aviation on cirrus cloud positive trends over congested air traffic regions. More specifically, the longitudinal distribution of cirrus cloud

trends from 1984 to 2004 was found to be positively correlated (+0.6) with the spatial distribution of aviation flown distance over the northern middle latitudes and not over the tropics. In the tropics over the regions studied, trends in cirrus cloud cover were found to be significantly correlated with trends in the vertical winds (–0.4) and with trends in relative humidity (+0.8).

5 ACKNOWLEDGMENTS

This study was conducted within the FP6 Integrated Project QUANTIFY (003893-GOCE) funded by EC. *NCEP Reanalysis data were provided by the NOAA/OAR/ESRL PSD, Boulder, Colorado, USA, from their web site at* http://www.cdc.noaa.gov/.

REFERENCES

Eleftheratos, K., C.S. Zerefos, P. Zanis, D.S. Balis, G. Tselioudis, K. Gierens, and R. Sausen, 2007: A study on natural and manmade global interannual fluctuations of cirrus cloud cover for the period 1984–2004. *Atmos. Chem. Phys. 7*, 2631–2642.

Gierens, K., 2007: Contrails, contrail cirrus, and ship tracks. *Proceedings of the TAC-Conference*, June 26 to 29, 2006, Oxford, UK, 214–220.

Krebs, K., 2006: Analyse des Einflusses des Flugverkehrs auf die natürliche Zirrusbewölkung über Europa, Nordafrika und dem Nordatlantik. *Dissertation*, Ludwing-Maximilians Universität München, 211pp (in German).

Luo, Z., W.B. Rossow, T. Inoue, and C.J. Stubenrauch, 2002: Did the Eruption of the Mt. Pinatubo Volcano Affect Cirrus Properties?. *J. Climate 17*, 2806–2820.

Mannstein, H., and U. Schumann, 2005: Aircraft induced contrail cirrus over Europe. *Meteorol. Z. 14*, 549–554.

Mannstein, H., and Schumann, U., 2007: Corrigendum to "Aircraft induced contrail cirrus over Europe". *Meteorol. Z. 16*, 131–132.

Minnis, P, J.K. Ayers, R. Palikonda, D.R. Doelling, U. Schumann, and K. Gierens, 2001: Changes in cirrus cloudiness and their relationship to contrails. *Proceedings American Meteorology Society*, Boston, USA, No. 11.9, 239–242.

Minnis, P., J.K. Ayers, R. Palikonda, and D. Phan, 2004: Contrails, Cirrus Trends, and Climate. *J. Climate 17*, 1671–1685.

Rossow, W.B., and R.A. Schiffer, 1999: Advances in understanding clouds from ISCCP. *Bull. Amer. Meteor. Soc. 80,* 2261–2287.

Sausen, R., I. Isaksen, V. Grewe, D. Hauglustaine, D.S. Lee, G. Myhre, M.O. Köhler, G. Pitari, U. Schumann, F. Stordal, and C. Zerefos, 2005: Aviation radiative forcing in 2000: An update on IPCC (1999). *Meteorol. Z. 14*, 555–561.

Schumann, U., 1996: On conditions for contrail formation from aircraft exhausts. *Meteorol. Z. 5*, 4–23.

Schumann, U., 2005: Formation, properties and climatic effects of contrails. *Comptes Rendus Physique 6*, 549–565.

Stordal, F., G. Myhre, E.J.G. Stordal, W.B. Rossow, D.S. Lee, D.W. Arlander, and T. Svendby, 2005: Is there a trend in cirrus clouds cover due to aircraft traffic?. *Atmos. Chem. Phys. 5*, 2155–2162.

Stubenrauch, C.J., W.B. Rossow, F. Cheruy, A. Chedin, and N.A. Scott, 1999: Clouds as seen by satellite sounders (3I) and imagers (ISCCP), Part I, Evaluation of cloud parameters. *J. Climate 12*, 2189–2213.

Stubenrauch, C.J., and U. Schumann, 2005: Impact of air traffic on cirrus coverage. *Geophys. Res. Lett. 32*, L14813, doi: 10.1029/2005GL022707.

Zerefos, C.S., K. Eleftheratos, D.S. Balis, P. Zanis, G. Tselioudis, and C. Meleti, 2003: Evidence of impact of aviation on cirrus cloud formation. *Atmos. Chem. Phys. 3*, 1633–1644.

Zerefos, C.S., K. Eleftheratos, P. Zanis, D.S. Balis, and G. Tselioudis, 2007: Search for Man-Made Cirrus Contrails over Southeast Asia. *Terr. Atmos. Ocean. Sci. 18(3)*, 459–474.

Ice nucleation on soot in contrails and cirrus: laboratory view

O.B. Popovicheva*,
Institute of Nuclear Physics, Moscow State University, Moscow, Russia

P. J. DeMott, K. A. Koehler, S. M. Kreidenweis, M. D, Petters, C. M. Carrico
Department of Atmospheric Science, Colorado State University, Fort Collins, CO,USA

N.Shonija, E.Kireeva
Chemical Department, Moscow State University, Moscow, Russia

Keywords: aircraft particulates, soot, ice nucleation, contrail, cirrus

ABSTRACT: Laboratory studies of water uptake and ice nucleation (for temperatures ≤ -40ºC) are presented for combustion particles of a wide range of physico-chemical properties, from hydrophobic through a range of hydrophilicity, to hygroscopic ones. Different mechanisms of water interactions with aircraft-generated soot aerosols of various compositions are considered for contrail and cirrus formation conditions. The findings generally confirm that heterogeneous ice nucleation is a function of surface oxidation of hydrophilic soot, hydrophobic soot initiates the ice phase from water vapor only at water supersaturated conditions while hygroscopic soot behaves in a manner reflecting homogeneous freezing with particles containing soluble matter.

1 INTRODUCTION

The climate impacts of aircraft particulate emission is highly uncertain because of the poor knowledge of soot aerosols ability to influence cloud formation and thus soot lifetime with respect to nucleation scavenging and precipitation removal, as well as to affect cloud optical properties and radiative balance. Contrail observations supported by theoretical estimates based on simple models of plume evolution suggest that contrails only form at high relative humidities, when liquid saturation with respect to water is reached in the plume (Karcher et al., 1998). The specific ice nucleation activity of aircraft-generated soot particles and their impact on threshold contrail formation conditions is still an important open question. An estimate of the maximum number concentration contribution of aircraft–generated soot particles results in an increase of the potential ice nuclei (IN) number concentration of up to 50 % at the main aircraft flight altitude (Hendricks et al., 2005). A potentially strong soot indirect effect has also been inferred when including such additional numbers of heterogeneous freezing ice nuclei along with the predominant sulfate homogeneous freezing process in microphysical models of cirrus clouds (DeMott et al., 1997). However, the state of scientific understanding of microphysical and chemical processes at the surface of soot aerosols that cause ice nucleation is still poor. Contrail formation models assume ice nucleation on initially hydrophobic soot particles which require the activation by plume processing while hygroscopic properties are considered for BC aerosols in the global simulations (Hendricks et al., 2005). Long-term research progress requires the development of new concepts and laboratory approaches with respect to aviation-emitted aerosol impacts on ice cloud formation.

Advanced QUANTIFY (Popovicheva et al., 2008a) and previous PartEmis (Petzold et al., 2005) studies have proven the highly heterogeneous nature of aircraft-generated soot aerosols with respect to both physical (size, morphology, porosity) and chemical (composition, impurities) properties, in dependence on engine design, operation conditions, and fuel content. Data of different characterization campaigns shows the dominant mass of BC over organic and sulfates especially at high engine power (Herndon et al., 2007), H_2SO_4 coverage of a few monolayer at high fuel sulfur content, non-volatile OC at low combustion temperature (Petzold et al., 2005), and the high water soluble fraction (WSF) and many surface functionalities responsible for water interactions (Popovicheva et al.,

* *Corresponding author:* Olga Popovicheva, Institute of Nuclear Physics, Moscow State University, 119991, 119991, Moscow, Russia. Email: polga@mics.msu.su

2004). Moreover, examination of characteristics of soot collected at background testing facilities for typical engines showed a main fraction of soot with low O, S content, probably relating to hydrophobic particles, and a fraction containing impurities with high O,S, Fe content which may be assigned to hydrophilic or even hygroscopic particles (Popovicheva et al., 2004). Therefore we may conclude that aircraft engine generates soot aerosols with properties which may vary from hydrophobic, through hydrophilic to hygroscopic, in dependence on surface chemistry and amount of hydrophilic impurities.

This work reports the laboratory measurements of water uptake and ice nucleation on various characterized soots with a wide range of physico-chemical properties. Different ice nucleation behaviors depending on temperature and soot particle hydrophilicity reflect a variety of particle interactions with water at low temperatures. These studies contribute toward clarifying the relationship between the extent of soot hydrophilicity and IN activated fraction at atmospheric conditions. Fractions of hydrophobic, hydrophilic and hygroscopic soot particles predicted to activate within a plume at contrail formation conditions are reported with the purpose of relating these to general observations of the contrail formation conditions. Also, the apparent range of soot hydrophilicity that is most favorable for heterogeneous ice nucleation at the cirrus formation conditions is proposed.

2 WATER UPTAKE QUANTIFICATION

Quantification of atmospheric impacts stemming from water interactions with soot particles of various origin, including emitted from aircraft engines, requires identification of hydrophobic and hydrophilic soots. Therefore, water uptake measurements are performed in laboratory on well-characterized soots available for atmospheric studies (Popovicheva et al., 2008a). Differing characteristics were achieved through generation by three different combustion sources; three soots from natural gas pyrolysis and soot from a turbulent diffusion flame in an aircraft engine combustor. Comparative analysis of water adsorption isotherms on soots of various compositions allows suggesting a concept of quantification (Popovicheva et al., 2008b). Systematic analysis demonstrates two mechanisms of water/soot interaction, namely, the bulk dissolution into soot water soluble coverage (absorption mechanism) and the water molecule adsorption on surface active sites (adsorption mechanism). Water uptake on hygroscopic soot takes place by the absorption mechanism: it significantly exceeds the formation of many surface layers. If soot particles are made mostly from elemental carbon and/or have a water insoluble organic coverage, they are classified as non-hygroscopic. Low water adsorption on some active sites following cluster formation is a typical mechanism of water interaction with hydrophobic soot. If the water film extending over the surface is formed due to cluster confluence it is suggested that soot is hydrophilic.

Thermal soot (TS) particles produced from natural gas combustion are classified as hydrophobic with a surface of low polarity. Graphitized Thermal soot (GTS) particles are proposed for comparison as extremely hydrophobic and of very low surface polarity. In contrast, oxidation of TS soot leads to an increase in the density of active water adsorption sites and the extent of surface polarity, thus to production of hydrophilic Thermal Oxidized soot (TOS). Aircraft engine soot (AEC), produced from burning TC1 kerosene in a gas turbine engine combustor, exhibit hygroscopic properties. Due to the presence of water soluble organic and inorganic material (near 3.5% sulfates) many AEC particles can be covered by water layers even below water saturation conditions.

3 ICE NUCLEATION ON SOOT

The present study seeks direct evidence for IN activity at environmentally-relevant water supersaturations and for ice nucleation behaviours at contrail and cirrus formation conditions, using this set of soots of varying and well-characterized physical and chemical characteristics. Laboratory measurements of ice nucleation were performed at conditions that simulate those in the atmosphere; a continuous flow diffusion chamber (CFDC) was used to scan the relative humidity conditions needed for IN activation at temperatures typical for the upper troposphere (down to -600C) (Koehler et al., 2009). Soot was dispersed using a fluidized bed generator and then size-selected by the DMA prior to being introduced to the CFDC.

Hydrophobic TS soot particles, having some active sites for water adsorption, may activate ice nucleation at -40 ºC only in the water supersaturated regime (see for details Koehler et al., 2009). A strong increase in the nucleated fraction, up to 10% of the particles frozen, occurred only above ~102% RH_w. At -57 °C, ice nucleation occurs on a small fraction (<1 in 1000) of TS soot starting at $RH_w < RHKoop$. Heterogeneous freezing appears as the most likely explanation for small ice nucleated fraction at RH_w well below water saturation. Larger proportions of the 200 nm than the 100 nm particles are typically activated for the same T and RH_w conditions.

Extremely hydrophobic GTS soot particles with limited active sites are observed to initiate the ice phase only at water supersaturated conditions, RH_w>102%, at both -40 and -51.5 °C . Ice nucleation did not occur until the particles were exposed to water supersaturations approaching presumably those high enough to condense water onto the particles. Ice formation was observed only on ~1% of the particles at up to several percent water supersaturation. Although onset of detectable ice formation was observed at a slightly lower RH_w at -51 °C than at -40 °C, similar activated fractions were observed at both temperatures.

The fraction of particles initiating ice formation is shown in Figures 1,2 for hydrophilic and hygroscopic soot particles, respectively. The sizes of dry particles and the scheme of specific water interaction (at left) are included in the figures. The "Koop lines (KL)" in each figure indicate the conditions for which homogeneous freezing of 200 nm ammonium sulfate particles is predicted for the CFDC residence times. Hydrophilic TOS particles have many active sites which may grow water clusters and form the water film on the surface; 200 nm TOS particles display onset ice nucleation conditions close to RH_{Koop} at -40 ˚C (see Fig.1). By 101% RH_w, the frozen fraction exceeds 20%. At -51.5 ˚C, 10^{-4} of the TOS particles activated by RH_w = 85%. More efficient ice nucleation occurring in this lower-RH regime, up to ~RH_{Koop} must proceed via a heterogeneous mechanism. In contrast to the behaviors of TS soot, however, ice formation on TOS particles displayed a steep increase in the region $RH_{Koop}<RH_w$ <100%, leading to activated fractions of TOS exceeding 10% by RH_w = 100%.

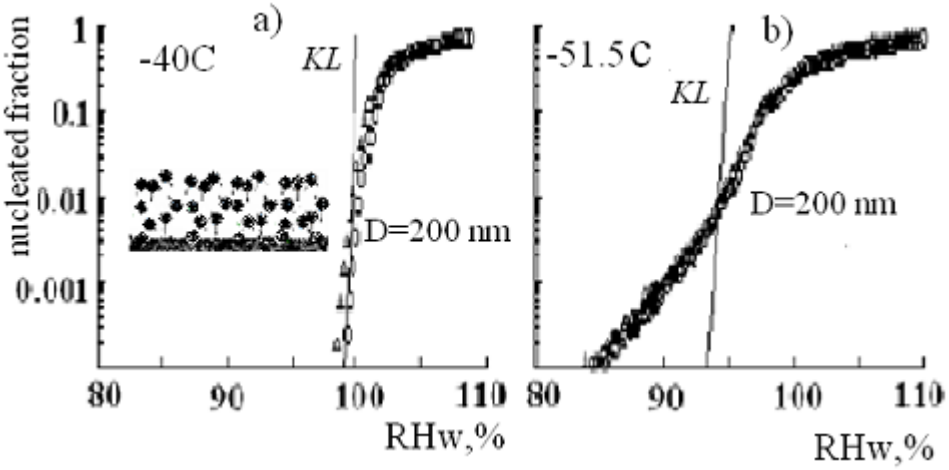

Figure 1. Ice nucleation of hydrophilic TOS soot particles at a) -40°C, b) -51.5°C.

Hygroscopic AEC soot activates ice formation at -40 ˚C near the predicted point for homogeneous freezing of pure dissolved solute (see Fig.2). More than 10% of the particles froze for RH_w = 102%. Similarly, at -57 ºC, both 250 nm size-selected particles and the polydisperse particle distribution showed significant increases in ice nucleated fraction near the homogeneous freezing nucleation threshold. In comparison to the non-hygroscopic soot particles, the AEC particles nucleated ice several to ten times more efficiently at -40 and -57 ºC for $RH_w > RH_{Koop}$, with ~4% of particles frozen at water saturation and 10% frozen at 102% RH_w in both cases. These observations appear at least consistent with the dissolution of water in the soluble coverage of a large fraction of these particles, leading to homogeneous freezing, while the other fraction may be less hydrophobic.

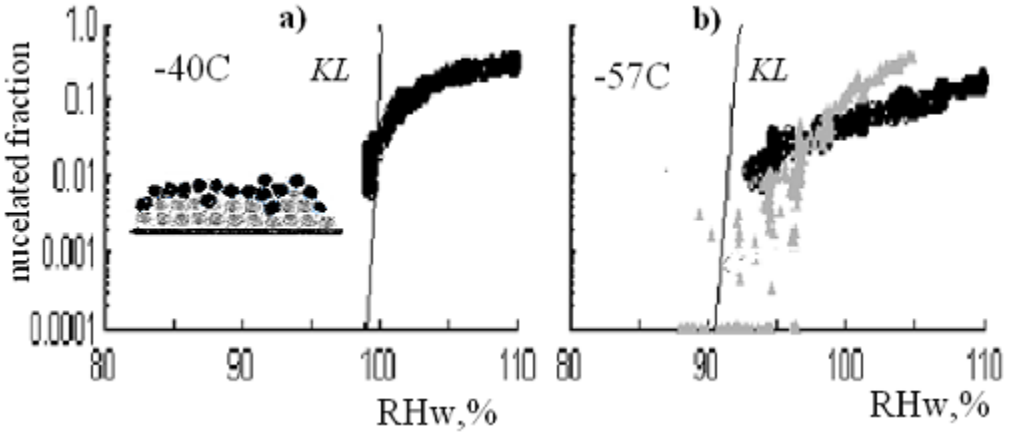

Figure 2. Ice nucleation of hygroscopic AEC soot particles at a) -40°C, b) -57°C.

4 CONTRAIL AND CIRRUS FORMATION

Experimental results suggest that the ability of soot particles of various physico-chemical properties to act as freezing nuclei in the atmosphere is related to their mechanism of interaction with water vapor. Specifically, processes that promote water uptake can facilitate ice nucleation at cirrus temperatures. This finding may be applied for aircraft contrail and cirrus formation with the hypothetical assumption that aircraft engines generate and emit into the atmosphere soot particles with a spectrum of hygroscopic properties.

Thus, we apply the obtained data for an aircraft plume situation assuming three different type of soot particle emitted and the CFDC RH uncertainty of 3%: hydrophobic, hydrophilic and hygroscopic as schematically shown in Figure 3. In the plume soot particles with different extents of hydrophilicity interact with water in accord with their water absorbability, and at the moment water saturation is exceeded we may conclude that about 10 to 50% of hydrophilic particles can freeze heterogeneously, at least 4 to 20% of hygroscopic particles (taking into account the example of AEC soot) may homogeneously freeze, and virtually no ice nucleation would occur on hydrophobic particles. At least 10% water supersaturation is needed to activate all hydrophilic particles and possibly more to freeze high proportions of hydrophobic aerosols. In general, this scenario is in accord with previously observations indicating that water saturation is needed for contrail formation whenever ice crystals are formed on exhaust soot (Karcher et al., 1998). Below water saturation very small numbers of soot particles may act as IN but significantly above water saturation all emitted soot aerosols of any surface properties have to serve as nuclei for contrail formation.

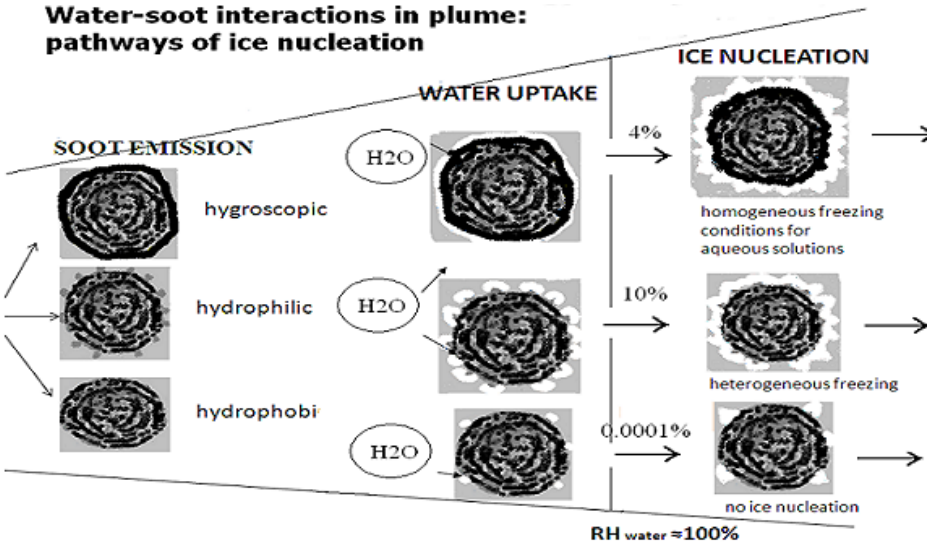

Figure 3. Scheme of pathways of ice nucleation on soot emitted in aircraft plume.

If we consider the effects of the possible physico-chemical nature of soot aerosols and order of magnitude number concentration estimates of BC in the atmosphere we can assume that hydropho-

bic soot particles should not alter cirrus cloud formation due to requiring high water supersaturations for ice nucleation at temperatures below -40 ºC. For soot particles that have developed a surface coverage of significant amounts of water soluble material, ice nucleation may be limited to occurring only at relative humidities near to or exceeding values required for homogeneous freezing of similar sizes of soluble particles in the upper troposphere. Their freezing is then indistinguishable from that of other particles containing water soluble species and they must compete with these other particles. Only special circumstances could allow hygroscopic soot particles to alter cirrus properties by acting as centres for homogeneous freezing. This could occur in situations where soot particles dominate aerosol numbers overall or especially at larger particle sizes. In this case, they would be the first ones to freeze in the homogeneous freezing regime, but cloud microphysical and radiative properties might not be altered.

A greater impact on cirrus formation and properties is expected if soot particles act as heterogeneous ice nuclei at lower RH_w than required for homogeneous freezing. In this case, the number concentration of ice nuclei required to dominate ice formation in competition with homogeneous freezing depends on the dynamics (updraft) driving cirrus formation. Below -40 ºC and below RH_{Koop}, ice formation occurred within 1 in 100 oxidized soot particles. Considering previous parcel modeling studies (DeMott et al., 1997), background upper tropospheric soot concentrations of 0.1 to 1 cm^{-3} would be predicted to have no impact to very modest impacts on natural cirrus formation if 10^{-4} to 10^{-2} fractions of the particles serve as freezing nuclei at $RH_w < RH_{Koop}$. These impacts would be restricted to cloud formation in the synoptic scale regime of vertical motions (under several cm s^{-1}), and are not expected for the stronger mesoscale motions present in cirrus generating cells. However, depending on the type of soot present or its transformation through oxidative processing, the impact of heterogeneous freezing nuclei on cirrus formation could be quite significant for higher soot concentration scenarios, such as those that occur when cirrus form in air masses affected by aged aircraft exhaust plumes or biomass smoke plumes.

5 CONCLUSIONS

Ice nucleation behaviors in relation to water uptake were investigated for soots whose properties ranged from hydrophobic to hygroscopic at the conditions of contrail and cirrus formation. It is found that hydrophobic soot initiates the ice phase from water vapor only at water supersaturated conditions while hydrophilic soot with oxidized surface and hygroscopic soot with a soluble coverage display ice nucleation onset at slightly lower conditions, in general agreement with with contrail formation observations. Based on current results, hydrophobic soot may not impact ice nucleation in atmosphere, while highly hygroscopic soot should mimic the homogeneous ice nucleation behaviors of any other hygroscopic particles in the upper troposphere. Surface polarity of hydrophilic soots from various combustion sources (including aircraft) is considered to support the most effective heterogeneous ice nucleation mechanism by ice germ growth on hydrophilic nucleation sites in cirrus clouds forming below water saturation.

ACKNOWLEDGEMENTS

This study was supported by the EC within the Integrated project QUANTIFY (Contract No.003893 GOCE), Project ISTC 3097. Partial support was also provided by the National Aeronautics and Space Administration under Grant #NNG06GF00G, the U.S. Department of Energy's Office of Science (BER) through the Western Regional Center of the National Institute for Climatic Change Research (Contract #MPC35TA-A1) and the U. S. National Science Foundation via Grant ATM-0521643.

REFERENCES

DeMott, P. J., D. C. Rogers and S. M. Kreidenweis, 1997: The susceptibility of ice formation in upper tropospheric clouds to insoluble aerosol components. *J. Geophys. Res.* ,102, 19575-19584.

Hendricks, J., B. Karcher, U.Lohmann, and M.Ponater, 2005 :Simulating the global atmosphere black carbon cycle : a revisit to the contribution of aircraft emissions. *Geophys. Res. Lett*., 32, L12814,doi:10.1029/2005GL022740.

Herndon.S.C., T.B.Onasch,J.T.Jayne, E.C.Wood, P.E.Yelvington, J.Wormhoudt, M.J.Northway, P.Mortimer,D.R. Worshop M.S.Zahnizer, D.D.Nelson, J.H.Shorfter, J.B.McManus and R.C. Miake-Lye. Aircraft emission characterization. in R.Sausen, et al.(eds): *Proceedings of an International Conference on Transport, Atmosphere and Climate (TAC)*, Luxenburg: Office for Official Publications of the European Communities, ISBN 92-79-045583-0, 320pp.

Karcher, B. ,R. Busen, A. Petzold, F. P. Schroder, U. Schumann and E. J. Jensen, 1998:Physicochemistry of aircraft-generated liquid aerosols,soot, and ice particles-2.Comparison with observations and sensitivity studies.*J. Geophys. Res.,* 103, 17129-17147.

Koehler, K., P. DeMott, S.Kreidenweis, O. Popovicheva ,M. Petters, C.Carrico, E. Kireeva,T. Khokhlova, N.Shonija, 2009: Cloud condensation nuclei and ice nucleation activity of hydrophobic and hydrophilic soot particles. *Phys. Chem. Chem*., 11, 7906 – 7920.

Petzold A., Gysel M., Vancassel, Hitzenberger R., Puxbaum H., Vrochticky S., Weingarnter E., Baltensperger U., and Mirabel P.,2005: On the effect of organic matter and sulfur-containing compounds on the CCN activation of combustion particles, *Atmospheric Chemical Physics*, 5, 3187-3203.

Popovicheva, O.B., N.M., Persiantseva, E.E., Lukhovitskaya, N.K., Shonija, N.A. Zubareva, B. Demirdjian, , D.Ferry, and J. Suzanne, 2004: Aircraft engine soot as contrail nuclei. *Geophys. Res. Lett*., 31. L11104. doi:10.10029/2003GL018888.

Popovicheva, O. B.,N. M. Persiantseva, N. K. Shonija, P. DeMott, K. Koehler, M. Petters, S. Kreidenweis, V. Tishkova, B. Demirdjian and J. Suzanne, 2008: Water interaction with hydrophobic and hydrophilic soot particles. *Phys. Chem. Chem. Phys*., 10, 2332-2344.

Popovicheva, O.B., Persiantseva, N.M., Tishkova, V., Shonija, N.K., and Zubareva, N.A., 2008b. Quantification of water uptake by soot particles. *Environmental Research Letters* 3, doi:10.1088/1748-9326/3/2/025009

Detection of young contrails – selected results from the CONCERT (CONtrail and Cirrus ExpeRimenT) campaign

C. Voigt [*,**], U. Schumann, T. Jurkat, D. Schäuble, H. Schlager, M. Lichtenstern, M. Scheibe, T. Hamburger, A. Petzold, F. Arnold[***], A. Dörnbrack, F. Holzäpfel
Deutsches Zentrum für Luft- und Raumfahrt (DLR) – Institut für Physik der Atmosphäre Oberpfaffenhofen, Germany

[**] also at *Johannes-Gutenberg-Universität, Institut für Physik der Atmosphäre, 55099 Mainz, Germany*
[***]also at *Max-Planck Institut für Kernphysik, Atmospheric Physics Division, Heidelberg, Germany*

J.-F. Gayet, C. Gourbeyre
Université Blaise Pascal Clermont Ferrand, LaMP UMR 6016 CNRS, 63177 Aubière, France

M. Krämer, M. Kübbeler, J. Meyer
Forschungszentrum Jülich, Institut für Chemie und Dynamik der Geosphäre, ICG 1, 52425 Jülich, Germany

J. Schneider, J. Schmale, H. Eichler, W. Frey, S. Molleker, S. Borrmann
Johannes-Gutenberg-Universität, Institut für Physik der Atmosphäre, 55099 Mainz, Germany

Keywords: contrail, aircraft emissions, optical depth

ABSTRACT: Large uncertainties remain in estimating the climate impact from contrails. In particular it is unknown, whether the aircraft type has an influence on contrail properties. Therefore, microphysical and radiative properties of contrails were detected with the DLR research aircraft Falcon during the CONCERT campaign in October/ November 2008. During 12 mission flights over Western Europe 22 contrails from 11 different aircraft were probed and the ice particle number density, size, extinction, contrail dimension as well as trace gas fields were measured. Here we focus on the 14 minutes sampling of the contrail of an A319. The 1 to 3 min old contrail was detected in the vortex regime. It was observed at an altitude of 10.6km and a temperature of 216K in ice subsaturated air (82%<RHI<98%). Particle concentration, extinction, and ice water content decrease within the sampling period due to contrail ageing and dilution. A vertical contrail depth of 122m has been estimated from the measurements and agrees with vortex descent simulations. Micro- and macro-physical contrail observations allow for the quantification of the contrail optical depth, playing a crucial role for the estimate of contrail radiative forcing.

1 INTRODUCTION

Contrails are produced through mixing of the hot and humid aircraft exhaust with the cold ambient air when saturation with respect to liquid water is reached. Ice may nucleate in the aerosol below the contrail formation threshold temperature (Schumann, 1996), whereby liquid plume particles compete with the exhaust soot for the formation of contrail ice crystals. If the ambient air is ice-supersaturated, the initially line shaped contrail will develop into a persistent contrail cirrus deck. Atmospheric and plume specific processes acting on different scales result in a variability of contrail properties that can be quantified using probability distribution functions (Kärcher et al., 2009). Lee at al., (2009) present a first attempt to include such a variability of contrail properties in global climate simulations. Including aircraft induced cloudiness, they derive a net median aviation raditive forcing in 2005 of 4.9% (2–14%, 90% likelihood range) of the total anthropogenic radiative forcing. Thereby, the key parameter in determining the climate impact from contrails is the contrail optical depth.

[*] *Corresponding author:* Christiane Voigt, Deutsches Zentrum für Luft- und Raumfahrt (DLR) – Institut für Physik der Atmosphäre, Oberpfaffenhofen, D-82234 Wessling, Germany. Email: Christiane.Voigt@dlr.de

The contrail optical depth τ can be calculated from the effective ice crystal radii, the number density, the ice water content (IWC) and the contrail depth. Still, in situ and remote sensing data on these micro- and macro-physical contrail properties in the vortex regime are sparse. Reasons for the lack of contrail data are that the detection of numerous small aerosol and ice particles with different refractive indices poses a challenge for accurate in situ measurements. Further, the resolution of satellite instruments often inhibits the observation of young contrails with ages of few minutes from space.

Few studies investigate microphysical properties of young contrails. Mean ice crystal effective radii derived from in situ data show values of 0.5 to 1µm initially (Heymsfield et al., 1998), increasing due to condensation to values of up to 5µm at 30min contrail age (Schröder et al., 2000). Mean ice crystal concentrations larger than 1000cm^{-3} have been detected in 5 and 8s old contrails decreasing by dilution to concentrations of a few 100cm^{-3} (Schröder et al., 2000) or less than 100cm^{-3} (Febvre et al., 2009) over the first 3min of age. The ice water content in a range of 1 to 6mg m^{-3} in young contrails has occasionally been probed at temperatures near 218K (Schröder et al., 2000; Febvre et al., 2009). Arbitrary sampling of contrails in thin cirrus clouds at temperatures near 217K leads to IWC values of 1 to 3mg m^{-3} (Schäuble et al., 2009). Another study reports values of up to 18mg m^{-3} at 236K (Gayet et al., 1996). Contrail widths of 1 to 3km have been derived for less than 30min old contrails from Lidar measurements above Germany (Freudenthaler et al., 1995).

Given the sparsity of in situ measurements of contrail microphysical properties, here we report on a new set of contrail observations. The measurements were performed in November 2008 with the DLR research aircraft Falcon. During the CONCERT campaign (CONtrail and Cirrus ExpeRimenT) numerous contrails were sampled in ice sub- and supersaturated air (50<RHI<130%). In total 22 contrails from 11 different commercial airliners were probed, including an A380, several A340 and B737 and a number of smaller aircraft such as an A319. As the data evaluation is still ongoing, we focus here exemplarily on a 14 minutes sampling event of the contrail of an A319 above Northern Germany, which is suitable for statistical data analysis. We derive particle concentrations, ice water content, and contrail depth from our data and compare them to results from vortex descent simulations.

2 FALCON INSTRUMENTATION

Figure 1. Deployment of the DLR research aircraft Falcon during the CONCERT – campaign (CONtail and Cirrus ExpeRimenT) in October/November 2008.

During the CONCERT campaign a set of particle and trace gas instruments was deployed on the DLR research aircraft Falcon. The particle size distribution of large particles (20µm - 1mm) was detected with a 2DC probe, the particle shape (2.3µm pixel size) with a cloud particle imager (CPI)

and the scattering phase function of cloud particles (3µm - ~1mm) using a polar nephelometer (Gayet et al., 2006, Febvre et al., 2009). A forward scattering spectrometer (FSSP 300) probe detected the particle number density and size distribution of small particles in the size range 0.3 to 20 µm diameter (Petzold et al., 1997). The particle size distribution was evaluated assuming spherical particles and a refractive index of 1.33 for ice. During the first phase of the CONCERT campaign, an aerosol mass spectrometer (Schneider et al., 2006) was integrated in the Falcon instead of the FSSP.

The trace gas instrumentation consisted of a Lyman-α fluorescence Fast In situ Stratospheric Hgrometer FISH (Schiller et al., 2008) with a backward-facing inlet sampling water vapour with an uncertainty of 8%. In addition, nitric oxide and the sum of reactive nitrogen species NO_y were measured with a chemiluminescence instrument (Schlager et al, 1997) with an uncertainty of 8%. A chemical ionization ion trap mass spectrometer was operated to detect sulfur dioxide (SO_2) and nitrous acid HONO with an uncertainty of 30%. Contrails from different source aircraft were frequently probed with this instrumentation during the CONCERT campaign. Below we investigate data from a flight on 19 November 2008, where microphysical and chemical properties of the contrail of an A319 were measured for 14 minutes.

3 DETECTION OF CONTRAILS

Contrails were mainly probed above optically visible cirrus clouds, as this sampling strategy was found to be very effective. Predictions for high clouds or of the IWC from ECMWF analyses were used to send the aircraft into a cirrus region and the flight altitude was then adjusted based on contrail observations of the pilots. The contrail formation altitude was communicated to German Air Traffic Control, and commercial airliners flying in that region were asked to change their flight altitude to contrail formation altitudes. Then the Falcon was directed behind the airliners and contrails were detected at 5 to 85 nautical miles distance corresponding to contrail ages of 55 to 600s.

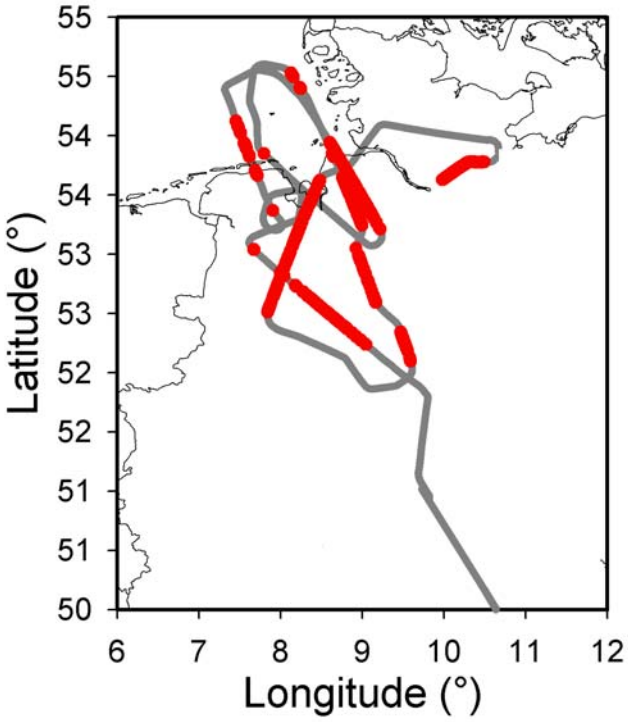

Figure 2, left panel. Flight path of the Falcon on 19 November 2009 (gray). Contrails are marked in red.

Figure 2, right panel. Photo of the contrail of the A319 which was probed by the instruments on the Falcon. The primary and the secondary wake, other contrails, and the nose boom of the Falcon can be seen.

On 19 November 2008 the Falcon five times probed the contrail of an A319, which was operating on that day exclusively as a contrail producing source aircraft. The Falcon took off in Oberpfaffenhofen, performed measurements within contrails above Northern Germany at altitudes between

10.1 and 10.8km and landed in Hamburg. The Falcon flight track, 5 contrail encounters of the A319 and contrail samplings of other aircraft are shown in Figure 2. Some contrail segments formed above cirrus clouds as seen on the photo in the right panel of Figure 2. Note that the primary and secondary wakes of the A319, contrails from other aircraft, and the nose boom of the Falcon are shown.

Measurements during the longest contrail penetration of 14 minutes from 53°N, 8°W to 54°N, 9°W are presented in Figure 3. Simultaneous peaks in the concentrations of reactive nitrogen, sulphur dioxide and particle number density are indications for a contrail encounter.

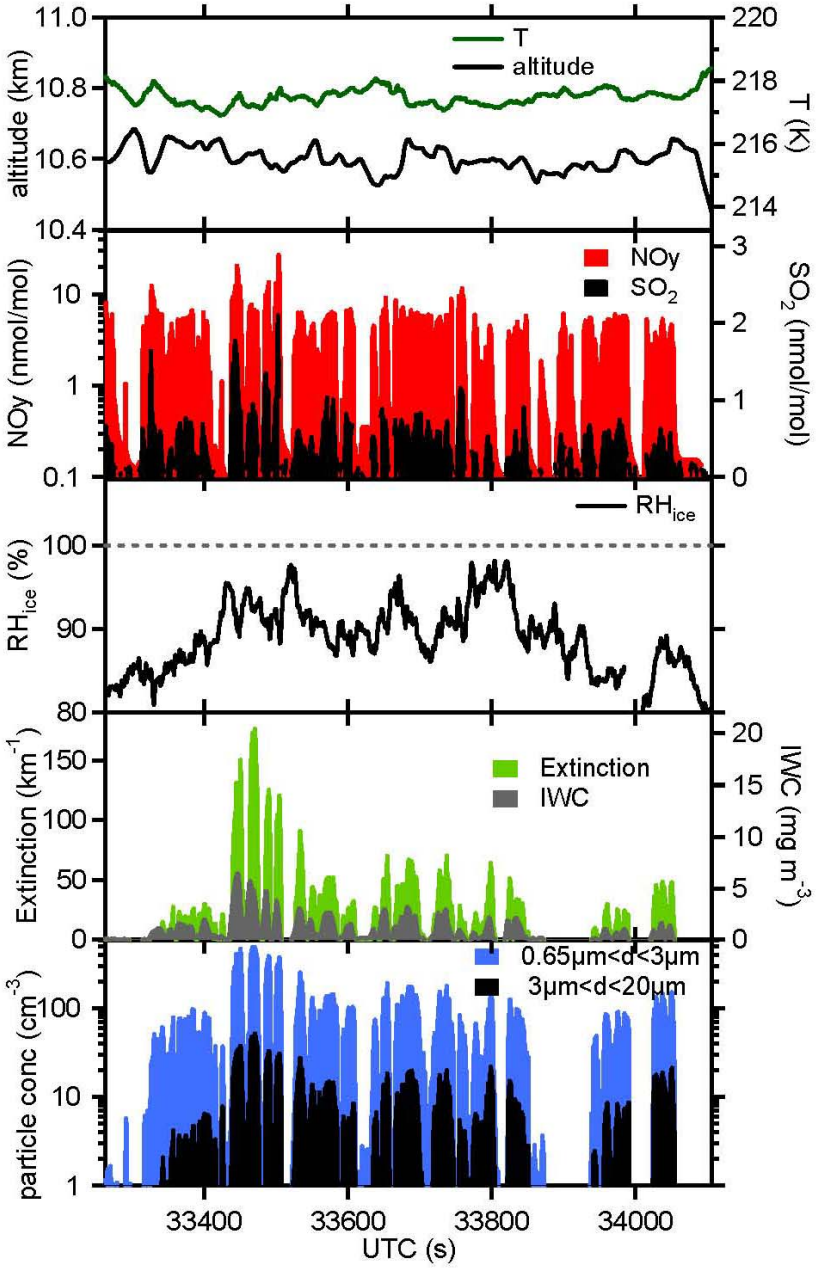

Figure 3. Sequence of 14 minutes of measurements in the contrail of an A319 performed on 19 November 2008 above Northern Germany. Temperature, altitude, trace gas mixing ratios of NO_y, SO_2 and RHI are shown in the upper three panels. The lower panels show contrail particle properties, i.e. the ice water content, the extinction of particles >3µm, and the particle concentrations in the cloud mode (3µm<d<20µm) and the haze mode (0.65µm<d<3µm). The contrail age increases from 77 to 184 s within the sampling sequence.

The contrail sequence was measured at an altitude of 10.6km and a temperature of 217.6K. Up to 27nmol/mol NO_y were observed in the contrail with average NO_y concentrations of 6nmol/mol. Such concentrations have been detected previously in the primary and secondary wake of aircraft (Schlager et al., 1997). SO_2 mixing ratios up to 2nmol/mol were measured with an average of

290pmol/mol and background concentrations of about 80pmol/mol. The air was slightly subsaturated with respect to ice (98>RHI>82%), suggesting that the contrail was evaporating.
Total ambient particle concentrations of up to 546cm^{-3} for particles in the size range 0.65<d<20µm have been detected by the FSSP. The particle concentration shows a substantial variability within the contrail and decreases within the measurement period due to dilution of the aging contrail. Particles >3µm exhibit an extinction up to 170km^{-1} decreasing with contrail age. The ice water content in the range of 7 to 1mg m^{-3} has been derived from a combination of FSSP and CIP data.
We calculated the age of the contrail from the positions of the Falcon and the A319 and meteorological parameters by matching the advected contrail with the Falcon flight path. The contrail was 77s old at the beginning of the sampling and 184s at the sampling end. Contrail dynamics for contrail with ages of 1 to 3min is described by the vortex regime.
Besides microphysical contrail properties such as particle number density, size and ice water content, we also evaluate contrail profiles and estimate the vertical contrail depth from our measurements. The data will allow us to derive the contrail optical depth.

4 CONTRAIL PROFILE

Engine emissions are captured by the wake vortices forming behind the aircraft. Due to momentum conservation, the primary vortices descent within the first 1 to 3min transporting a large fraction of the emissions including particles downwards. The air is adiabatically heated during its downward transport, which can result in a (partial) evaporation of ice particles in subsaturated conditions with respect to ice. A small fraction of the emissions including particles remains near its emission altitude in the secondary wake. Depending on ambient saturation ratios and descent depths, the primary and/or the secondary wake might survive the vortex phase and evolve into a persistent contrail. A profile taken in the A319 contrail near 33420s UT (101s contrail age) is shown in Figure 4.

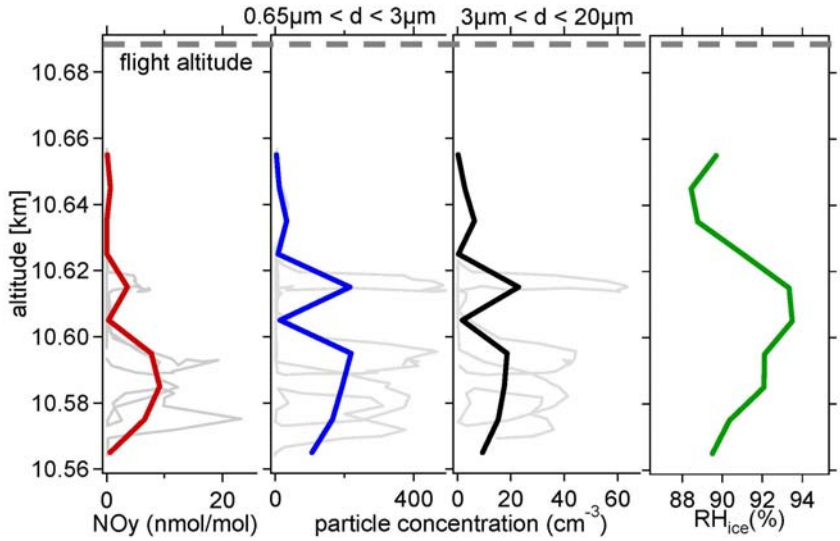

Figure 4. Profile of the NO_y mixing ratios, particle concentrations of the haze mode (0.65µm<d<3µm), the cloud mode (3µm<d<20µm), and RHI in the contrail of an A319 measured on 19 November 2008 at 33420 s UT. Thick lines are averages of the individual measurements (gray lines) in 10 m altitude intervals.

From the contrail profile, we estimate a vertical contrail depth of 122m, which is in agreement with simulations of the wake vortex descent of an A319 of 124m using the P2P model under standard ambient conditions (Holzäpfel et al., 2003).

5 CONCLUSIONS AND OUTLOOK

The CONCERT campaign provides an extensive and detailed data set on microphysical and optical contrail properties from 11 different aircraft, amongst them an A380, four A340, several B737, A319 and smaller aircraft. The data have been used for model validation (Schumann, 2009) The measurements of particle number density, size and contrail dimensions of the A319 will be used to derive contrail optical depths. Long sampling times in the contrail will allow for a statistical data analysis. The next step is to compare the contrail optical depths of the A319 to contrail samplings from other aircraft with the aim to investigate the the impact of aircraft type on contrail properties. The results including a statistical data analysis will appear soon in a refereed journal.

REFERENCES

Febvre, G., J.-F. Gayet, A. Minikin, H. Schlager, V. Shcherbakov, O. Jourdan, R. Busen, M. Fiebig, B. Kärcher, and U. Schumann, 2009: On optical and microphysical characteristics of contrails and cirrus, *J. Geophys. Res.,* 114, D02204, doi:10.1029/2008JD010184.

Freudenthaler, V., F. Homburg, and H. Jäger, 1995: Contrail observations by ground-based scanning Lidar: Cross-sectional growth, *Geophys. Res. Lett.,* 22, 3501–3504.

Gayet J.-F., V. Shcherbakov, H. Mannstein, A. Minikin, U. Schumann, J. Ström, A. Petzold, J. Ovarlez and F. Immler, 2006: Microphysical and optical properties of midlatitudes cirrus clouds observed in the southern hemisphere during INCA, *Q. J. R. Meteorol. Soc.,*132, 1-30.

Heymsfield, A. J., R.P. Lawson, and G.W. Sachse, 1998: Growth of ice crystals in a precipitating contrail, *Geophys. Res. Lett.,* 25, 1335–1338, 1998.

Holzäpfel F., 2003: A Probabilistic Two-Phase Wake Vortex Decay and Transport Model, *Journal of Aircraft,* 40, 2, 323-331.

Kärcher, B., U. Burkhardt, S. Unterstrasser, and P. Minnis, 2009: Factors controlling contrail cirrus optical depth, *Atmos. Chem. Phys., 9, 6229-6254*.

Lee, D., D. W. Fahey, P. M. Forster, P. J. Newton, R. C.N. Wit, L. L. Lim, B. Owen and R. Sausen, 2009: Aviation and global climate change in the 21st century, *Atmos. Environ.,* 43, 3520–3537.

Petzold, A., et al., 1997: Near-field measurements on contrail properties from fuels with different sulfur content, *J. Geophys. Res.*, 102, 29867–29881.

Schäuble, D., C. Voigt, B. Kärcher, P. Stock, H. Schlager, M. Krämer, C. Schiller, R. Bauer, N. Spelten, M. de Reus, M. Szakall, S. Borrmann,U. Weers, and T. Peter, 2009: Airborne measurements of the nitric acid partitioning in persistent contrails, *Atmos. Chem. Phys. Discuss.,* 9, 14165–14187.

Schlager, H., P. Konopka, P. Schulte, U. Schumann, H. Ziereis, F. Arnold, M. Klemm, D. Hagen, P. Whitefield, J. Ovarlez, 1997: In situ observations of air traffic emission signatures in the North Atlantic flight corridor, *J. Geophys. Res.,* 102, 10739-10750.

Schiller, C., M. Krämer, A. Afchine, N. Spelten, and N. Sitnikov, 2008: Ice water content of Arctic, midlatitude, and tropical cirrus, *J. Geophys. Res.,* 113, D24208, doi:10.1029/2008JD010342.

Schneider, J., S. Hings, N. Hock, S. Weimer, S. Borrmann, M. Fiebig, A. Petzold, R. Busen, B. Kärcher, Aircraft-based operation of an aerosol mass spectrometer: Measurements of tropospheric aerosol composition, *J. Aerosol Sci.,* 37, 839-857, doi: 10.1016/ j.aerosci.2005.07.002, 2006.

Schröder, F., B. Kärcher, C. Duroure, J. Ström, A. Petzold, J.-F. Gayet, B. Strauss, P. Wendling, and S. Borrmann, 2002: On the transition of contrails into cirrus clouds, *J. Atmos. Sci.,* 57, 464–480.

Schumann, U., 1996: On conditions for contrail formation from aircraft exhausts, *Meteorol. Z.,*5, 4 –23.

Schumann, U., 2009: A Contrail Cirrus Prediction Tool*, Intern. Conf. on Transport, Atmosphere and Climate*, Aaachen and Maastricht, EUR, in press.

Quantitative forecast model of contrail formation and prospects of its application

V.T. Dedesh*, R.Kh. Tenishev, S.N. Kiose, V.V. Popov, E.G. Pavlova, I.V. Voronich, M.A. Lavrov, V.P. Mogilnikov
Gromov Flight Research Institute (GFRI), Zhukovsky, Russia

A.I. Lanshin, A.A. Evstigneev
Baranov Central Institute of Aviation Motors (CIAM), Moscow, Russia

A.N. Nevzorov
Central Aerologic Observatory, Moscow, Russia

O.B. Popovicheva
Lomonosov Moscow State University (MSU), Moscow, Russia

Keywords: aircraft, contrails, cirrus clouds, forecast model

ABSTRACT: A complex methodic and quantitative model were developed for quantitative valuation and forecast of formation conditions and characteristics of contrails, in cruise flights of civil airplanes with different types of jet engines using specially equipped flying testbed Tu-154 prober/generator. The methodic uses uniform and 2D mixing of the exhaust engine jet and atmosphere. The data, obtained during the flight experiments proved the reliability of the methodic.

1 MOTIVATION

Influence of aviation on the environment is not limited only by the greenhouse gases. Contrail formation according to some researches can at least as important as CO_2. But in previous researches of contrails there were several aspects preventing us from clear understanding of the subject. First of all, characteristics of engine exhaust jet are appreciated by total heat equivalent and their values for given engines and airplanes are determined approximately. Then, peculiarities of bypass engines without mixing chamber and turboprop engines are not considered at all. Moreover, contrail formation conditions are considered only qualitatively, that prevents from direct influence estimation of deviations of engine and atmosphere characteristics on contrail characteristics and formation conditions.

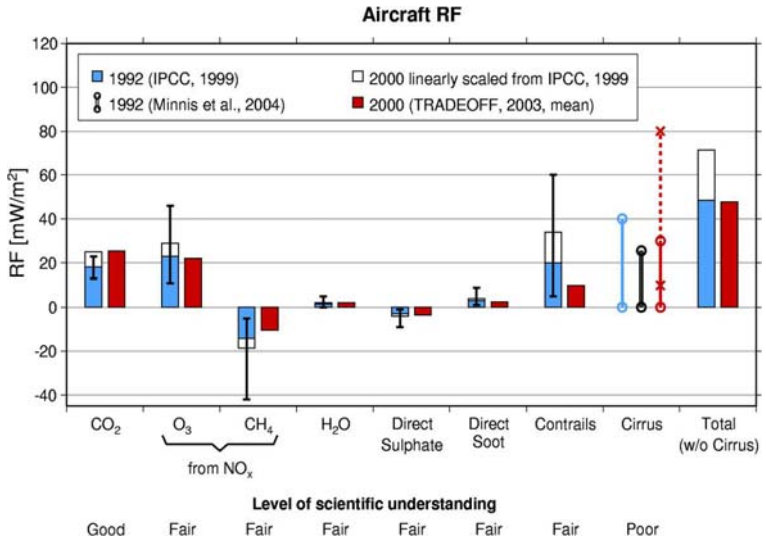

Figure 1. Radiative forcing from aircraft.

* *Corresponding author:* V.T.Dedesh, Gromov Flight Research Institute, 140182, Russian Federation, Moscow Region, Zhukovsky-2. Email: kd3@aha.ru

1.1 *The model*

Complex quantitative model was proposed. As a criteria of contrail formation and existence, index of maximum humidity supersaturation h_Σ is used, consisting of two parts: $h_\Sigma = h_m + e_{amb}$, where h_m = maximum supersaturation towards water while mixing exhaust jet with dry atmosphere, depending practically from engine characteristics, ambient temperature and pressure; and e_{amb} = atmosphere humidity on the flight altitude. The methodic, developed by the GFRI specialists differs in facts that engine exhaust jet characteristics are estimated directly from results of a special experiment or calculation and exhaust jet and atmosphere mixing is estimated with consideration of peculiarities of bypass engines and possible influence of engine flow-around at 2D mixing on equivalent mixing line while assuming uniform mixing of engine jet and atmosphere.

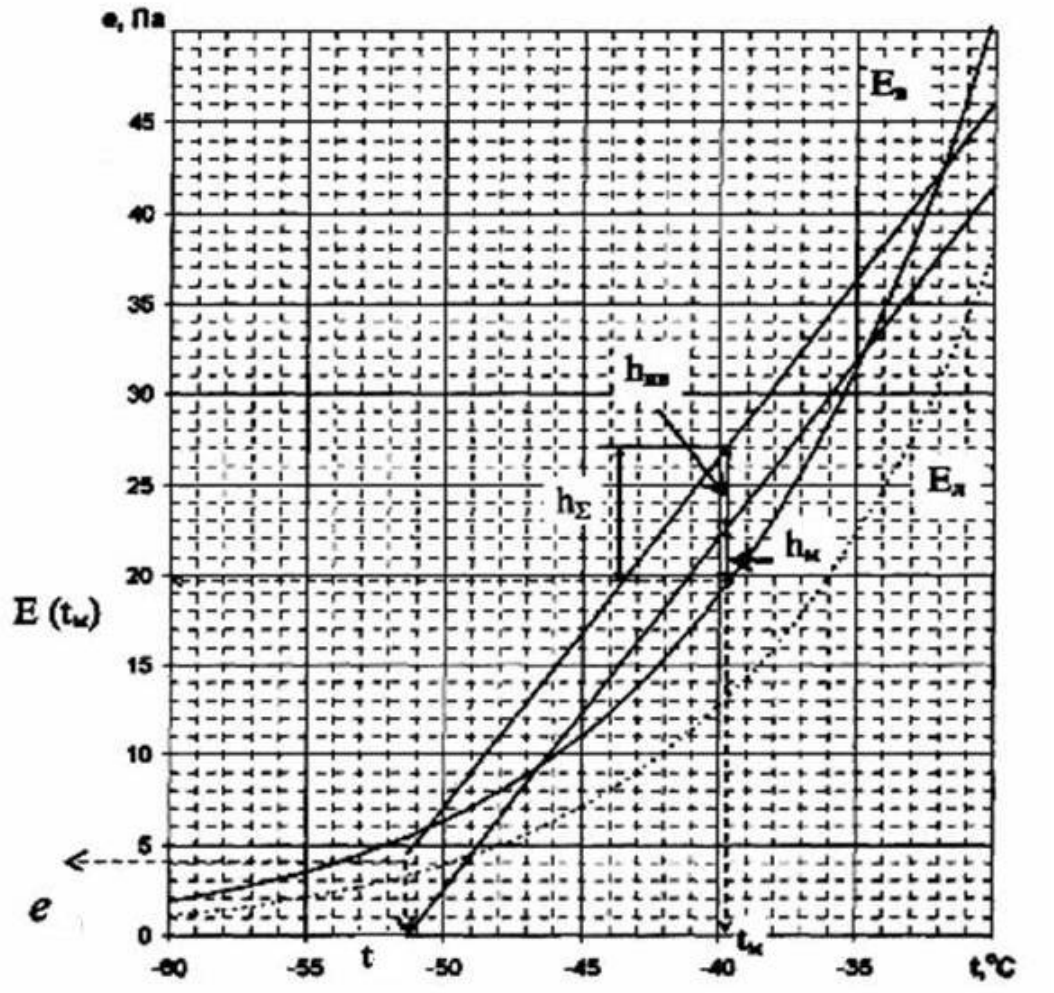

Figure 2. Quantitative supersaturation index.

1.2 *The testbed*

To prove the validity of the criteria and to adjust the methodic, flying testbed Tu-154 was used. It was equipped with special measuring means to measure cloud and contrail characteristics. The emphasis was done on the humidity of the air. It was measured by an aircraft condensation hygrometer (SKG) and by an on-board sorption hygrometer (BSIV). Water content of atmosphere and contrails was measured by the measurer of water content (IVOKS). Temperature values came from the resistance temperature detector (ET-17). For in-flight observation of condensation trail formation a periscope (TS-27AMSh) and a video camera were installed. For registration of formation borders and lifetime of condensation trails in solo and twin flights following devises are used: videotheodolitic system “Opal”, “Jantar” and also specialized camera for video and photo recording from earth.

Figure 3. Sensors on the flying testbed Tu-154M.

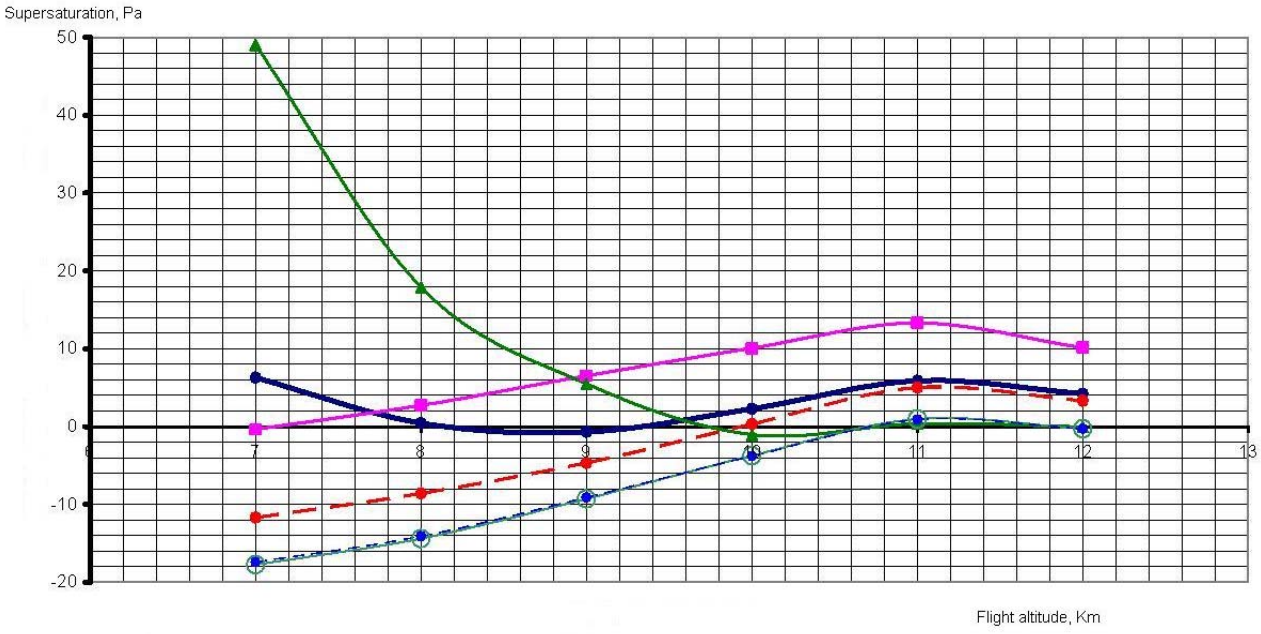

Figure 4. Calculation results for the D-30KU engine.

On the heights H = 7…8 km scatter of characteristics can be caused by higher temperatures of ambient air and their greater deviations from ISA standard or by greater range of margin values of humidity (partial pressure) between its saturations over water and ice. Above mentioned factors give more favourable conditions for carrying out experiments aimed at identification of the forecast model with supersaturation index $h_{\sum} = h_m + e_{amb}$ on formation and existence of contrails.

1.3 *The 2D model*

For examination of contrail formation processes of mixing of a jet from a modern bypass engine with concurrent flow a calculation methodic was developed. This methodic is based on solution of full system of gas dynamic equations considering turbulence. Main geometric and gas dynamic parameters are pointed out, physical and mathematical models of current are determined, calculation model is developed, technology of quantitative modelling is worked out.

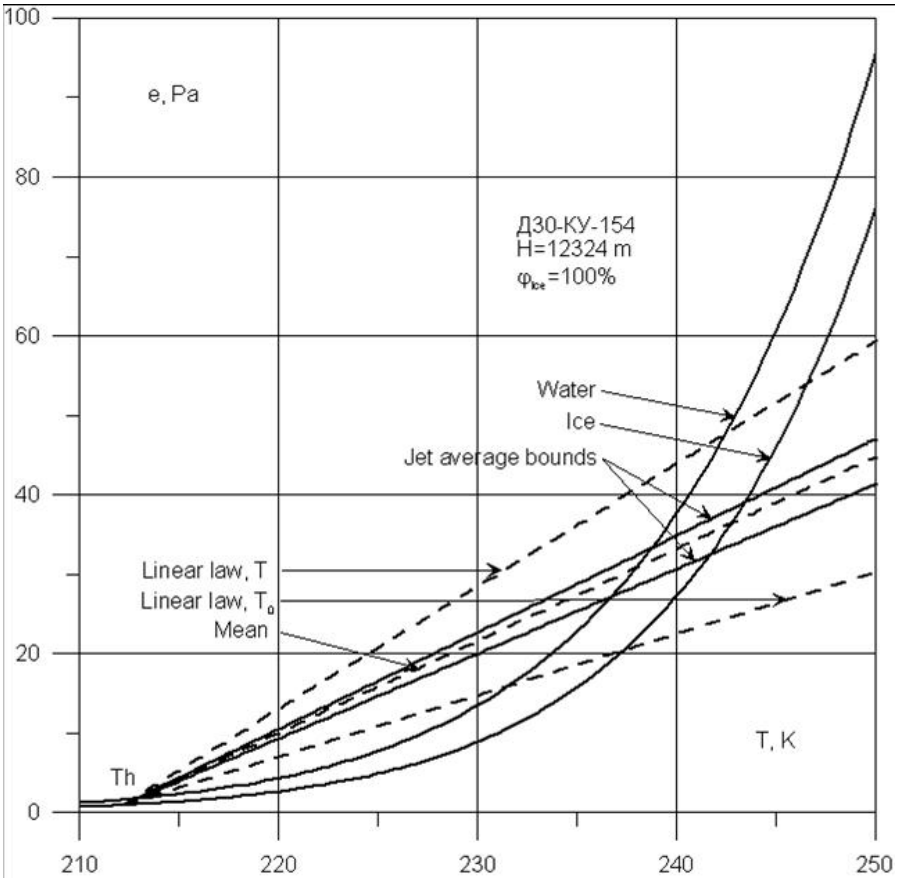

Figure 5. Uniform mixing line, calculated using 2D model.

Basing on these results, specification is done of quantitative forecast model of contrail formation conditions at uniform mixing of engine exhaust jet with atmosphere. Method of calculation mixing line gradient values is also proposed, considering both full and static temperatures of engine exhaust jet. Method of uniform mixing and methodic of calculation mixing line gradient values were used to calculate values of sum supersaturation index over water and ice considering both full and static temperatures of engine exhaust jet after engine mixing chamber.

$$B_0 = \frac{B_0(T^*_{mix}) + B_0(T_{mix})}{2} \qquad (1)$$

The conducted comparison showed that quantitative humidity supersaturation index calculated basing on the improved methodic, where average temperature in the mixing chamber ($T_{mix.av}$) is used, is more adequate to contrail formation conditions according to saturation curves over water and ice in comparison with the previous methodic ($T_{mix.abs}$) used up to the present.

According to engines without mixing chamber investigations of contrail formation conditions were also done. Research carried out using the developed model showed that averaged mixing line exists for engine with open fan.

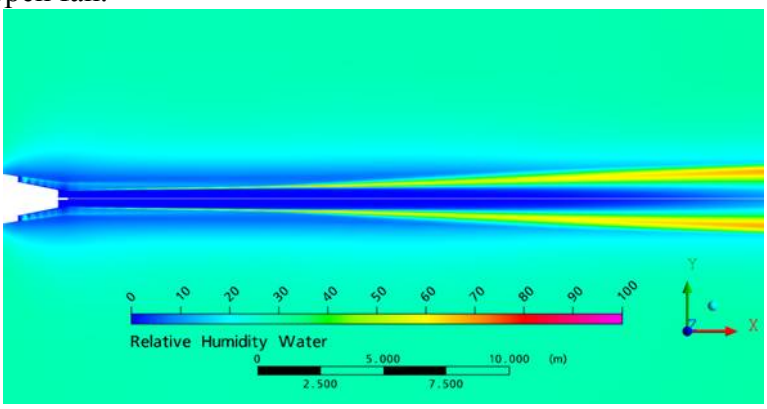

Figure 6. 2D calculation for engine with open fan.

2 RESULTS

The forecast model allows estimating characteristic and equivalent influence on h_Σ of engine characteristics and atmospheric pressure (flight altitudes); temperature and humidity on steady contrail formation conditions. Calculations of humidity supersaturation indexes h_Σ and its identification with experimental results showed that: two altitude borders of formation of steady contrails are possible for aircrafts flying in various air conditions. These borders depend from engine characteristics, temperature deviations from ISA temperatures $\pm 10^0$C; evaluation of equivalent influence in border region on high altitude can show change of the borders, where steady contrails can be formed, at changes of T_{amb}, ambient humidity and engine mode; in number of cases steady contrail formation was observed at $h_\Sigma < h_{\Sigma boundary}$ at $\Delta h_\Sigma = h_{\Sigma boundary} - h_\Sigma$, corresponding to the interval between saturation curves over water and ice ($\Delta e = e_{water} - e_{ice}$), that can be explained by presence of crystallisation centres (soot ,etc.)

Methodic of 2D mixing of engine jet and atmosphere is developed and tested on different engine types. It allows to estimate characteristics of mixing, including geometrical, averaging parameters, temperature Tmix and humidity in cross-sections.

Method is shown of calculating values of mixing line gradient (that can be used for calculating h_Σ) basing on the analysis of calculation of contrail formation conditions done for bypass jet engines with mixing chamber and open fan.

Using both T_4^* and T_{4stat} of jet engines with mixing chambers for estimation humidity supersaturation index is more adequate to contrail (ice particles) formation conditions and saturation curves over water and ice, than using only T_4^*. Calculations of humidity supersaturation indexes h_Σ using T_{mid} for bypass engines with mixing chamber and its identifications with results of experiment on the Tu-154 FTB with D-30KU engines showed that for these engines at boarder $h_\Sigma > 0$ contrails are steady.

$$T_{mid} \approx \frac{T_4^* + T_{4\,static}}{2} \tag{2}$$

$$B_0 = \frac{B_0(T_{mix}^*) + B_0(T_{mix})}{2} \tag{3}$$

3 CONCLUSION

The performed works and obtained results, when applied and developed, can essentially amplify works done in this field by specialists of European organisations. They are of great interest for ecological estimations of emission influence of specific aircrafts with different engines on contrail formation in cruise flights and possible influence on Earth climate, as well as for development of recommendations on flight organization on different routes (local, regional and international) with the object of reducing of this effect, considering peculiarities of atmosphere in specific regions, on specific air routes and in different seasons.

In case if characteristics of alternative fuels are available, it is also possible to use the methods developed to estimate their effect on contrail formation and existence during airplane cruise flights.

Conducted researches show that it is efficient to use the experience of complex researches and handling of jobs by different specialists according to consistent schedule in order to improve the efficiency of the further work.

4 ACKNOWLEDGMENTS

This work was partly funded by the International Science and Technology Center in the frames of the ISTC Project #3097.

REFERENCES

Dedesh V.T., R.Kh.Tenishev, N.A.Dankovtsev, A.P.Leut, E.G.Pavlova, A.N.Nevzorov, S.N.Kiose, V.V.Popov, A.I.Lanshin, 2005: Forecast and identification methodology of influence of jet engine characteristicson condensation trails formation in cruise flights, International conference Aircraft engines of the XXI century, CIAM, Moscow, Russia.

Dedesh V.T., R.Kh.Tenishev, N.A.Dankovtsev, A.P.Leut, E.G.Pavlova, S.N.Kiose, V.V.Popov, M.A.Grigoryev, A.N.Nevzorov, 2006: Need in developing flight research methodics of formation and existence of condensation trails of jet airplanes in cruise flights, Ninth international exhibition Engines-2006, ASSAD, Moscow, Russia.

Dedesh V.T., R.Kh.Tenishev, N.A.Dankovtsev, A.P.Leut, E.G.Pavlova, S.N.Kiose, V.V.Popov, A.I.Lanshin, M.A.Grigoryev, A.N.Nevzorov, 2006: GFRI experience in carrying out flight experiments on aircraft engines influence on atmospheric pollution, International aeronautics seminar Europe-Russia, Brussels, Belgium.

Fischter K., S.Markwart, R.Sausen, 2005: Influence of cruise flight altitude on condensation trails and corresponding radiational, Meteorologische Zeitschrift, vol. 14, No. 4,563-572.

Manstein G., U.Schumann, 2005: Cirrus clouds over Europe, formed by aircraft condensation trails, Meteorologische Zeitschrift, vol. 14, No. 15,549-554.

Mathes S., 2005: Impact of aviation on the environment in global scale, AERONEN III Work materials №17 Results of the seminar on air transport systems, Stockholm, Sweden.

Schumann U.,1996: On condensation trail of aircraft exhaust jet formation conditions, Meteorologische Zeitschrift, N.F. 5,4-23.

A Contrail Cirrus Prediction Tool

U. Schumann*
Deutsches Zentrum für Luft- und Raumfahrt (DLR) – Institut für Physik der Atmosphäre Oberpfaffenhofen, Germany

Keywords: contrails, contrail cirrus, simulation

ABSTRACT: An new "Contrail Cirrus Prediction Tool" (CoCiP) has been developed to simulate contrail cirrus resulting from a single flight as well as from a fleet of cruising aircraft, flight by flight, regionally or globally. The method predicts contrail cirrus for given air traffic and weather prediction data. The method describes the life cycle of each contrail individually using a Lagrangian Gaussian plume model with simple bulk contrail ice properties, without feedback to meteorology. Contrails are initiated when the Schmidt-Appleman criterion is satisfied and when the ambient atmosphere is humid enough to allow for contrail persistence. The initial plume properties reflect properties of the originating aircraft. The evolution of individual contrails of cruising aircraft is computed using wind, temperature, humidity, and ice water content from numerical weather prediction (NWP) output. The plume trajectory follows horizontal and vertical wind. The model simulates shear and turbulence driven spreading, ice water content as a function of ice supersaturation, and some ice particle loss processes (turbulent mixing, aggregation and sedimentation). Radiative cloud forcing is estimated for the sum of all contrails using radiative fluxes without contrails from NWP output. The tool is kept simple to allow for efficient contrail simulations. The method has been tested for case studies with some comparisons to observations. The most critical input parameter is the NWP humidity field. The results compare favourably with observations and support interpretations of insitu, satellite and lidar observed aviation impact on cirrus clouds. CoCiP can be used to predict and minimize the climate impact of contrails.

1 INTRODUCTION

Because of the general awareness of climate change and the growth of traffic, aviation caused environmental concerns which were discussed with respect to the fleet of civil aviation since the early 1990' (Schumann, 1994; IPCC, 1999). Despite considerable scientific progress in predicting the climate impact of aviation, still major uncertainties remain, in particular with respect to contrail cirrus (IPCC, 2007; Lee et al., 2009). The range of radiative forcing form present aviation induced contrails scatter by a factor of larger ten (from 3 to 120 W/m^2). Observed increases in cloudiness may be attributed to aviation, but the observations miss physical explanation and other explanations cannot be ruled out. Contrail and cirrus formation is a highly nonlinear process. The contrail cirrus formation depends strongly on the scale transition from the plumes with fresh soot and young contrails into spread cirrus layers. Early studies concentrated on line-shaped contrails, but contrails develop dynamically into cirrus at time scales of hours during which the line-shaped structure is lost. This scale transition requires a model that follows the history of all the contrails from the global fleet of aircraft from origin shortly after engine exit until the end of their lifetime due to sublimation or sedimentation. This paper describes a recently developed model for this purpose. The model is based on a Gaussian plume model as suggested a long time ago (Schumann and Konopka, 1994).

* *Corresponding author:* Ulrich Schumann, Deutsches Zentrum für Luft- und Raumfahrt (DLR) – Institut für Physik der Atmosphäre, D-82234 Oberpfaffenhofen, Germany. Email: ulrich.schumann @dlr.de.

2 THE MODEL

The contrail cirrus prediction (CoCiP) model is designed to analyze and predict contrail cirrus cover and the related radiative forcing from air traffic. The model simulates contrail cirrus resulting from a fleet of cruising aircraft, flight by flight, regionally or globally. The concept is illustrated by an example, see Figure 1.

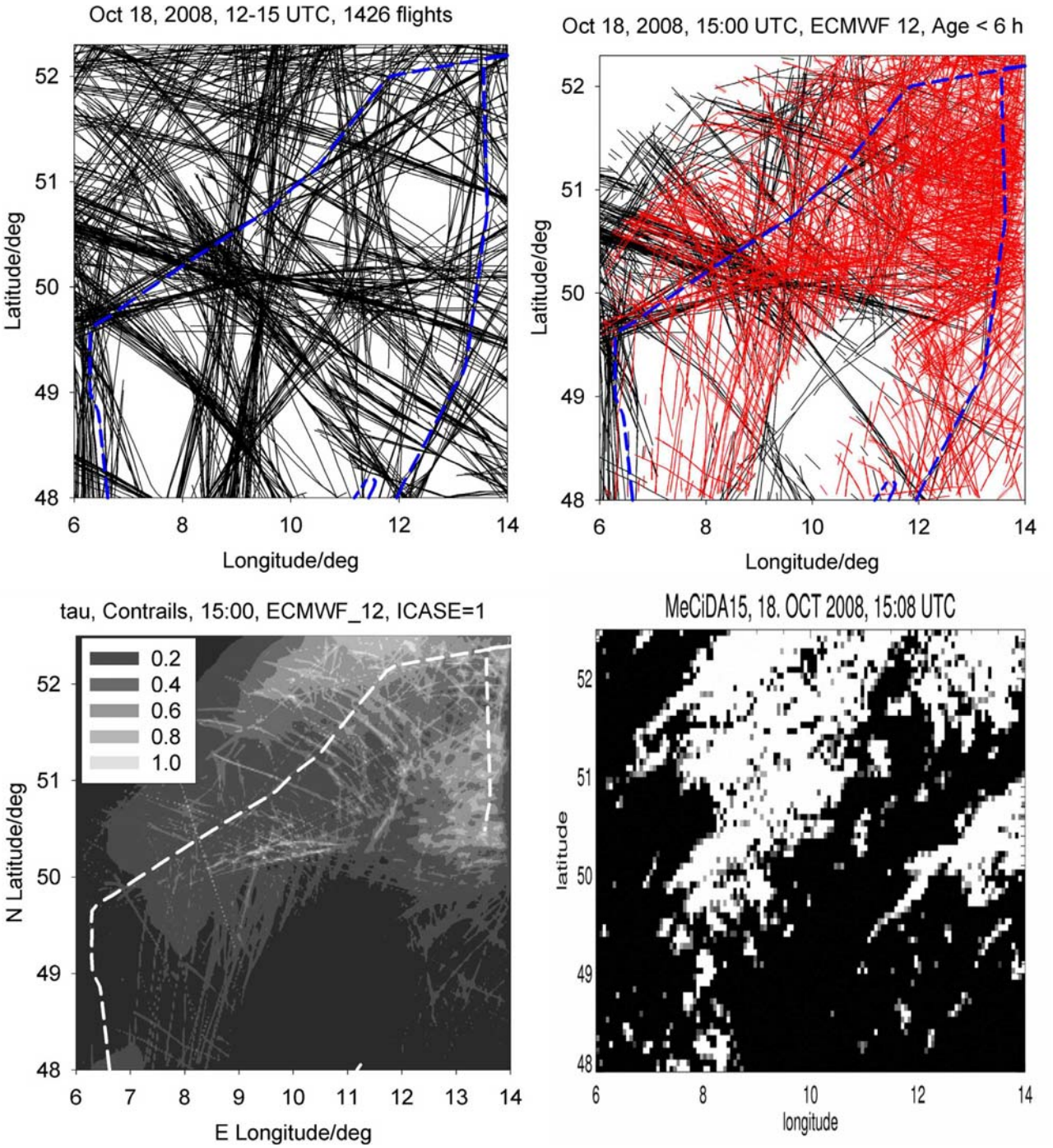

Figure 1. Example CoCiP output: Contrail pattern as computed for a 8°×4.2° (680×470 km2) region over Germany, for a case study (Oct 18, 2008, 15 UTC), for which contrails were observed visually and by lidar measurements with the Falcon research aircraft (flight path shown as blue or white dashed curve). Top left: flight paths of air traffic from all 1426 flights above 7.3 km altitude (FL 240) over Germany between 13 and 15 UTC that day. Top right: Flight segments causing contrails during recent 6 h which contribute to contrail cover at 15 UTC (black), and contrail plumes centre line (full red) together with their left and right boundaries (dashed red; closely near the centre lines). Bottom left: solar optical depth of these contrails (from CoCiP) superposed on cirrus (from ECMWF output). Bottom right: Cirrus cloud cover (white) computed by K. Graf with the MeCiDa algorithm (Krebs et al., 2007) from Meteosat data at the given time.

The method computes the contrail cirrus cover for a given time instant for given weather data and for given data of air traffic for the past covering all contrails with life times of up to six hours (in Fig 1) or about a day (for larger domains). The model requires input in terms of wind vector, temperature, humidity, and ice water content fields as available from numerical weather prediction (NWP) or climate model output, as a function of time and three dimensions (3d) in space (typical time intervals: 1-3 h; typical spatial resolution: 0.25-1 degree horizontally, 20 levels vertically from 120-500 hPa for Gemany). In addition, the model requires the irradiances for outgoing longwave radiation (OLR) and short-wave reflected radiation (RSR) at top of the atmosphere (TOA) as a function of horizontal coordinates and time. The traffic data need to be provided, flight by flight, as waypoint sequences (3 space coordinates and time) together with the aircraft type. The tool is kept simple to allow for efficient global contrail simulations. The example requires about 10 s computing time on a single processor Laptop.

The model treats each exhaust plume as a Gaussian plume (Konopka, 1995; Schumann et al., 1995; Dürbeck and Gerz, 1996). The model assumes that any mass specific concentration c in the plume has the distribution $c(x,y,z,t)= (C_0/A) \exp(-(1/2)\mathbf{x}^T\boldsymbol{\sigma}^{-1}\mathbf{x})$, where C_0 is the mass per unit length in the contrail, A is the plume cross-section area, $\mathbf{x}$ is the vector of space coordinates relative to the plume centre ($\mathbf{x}$=(x,y,z), x in flight direction, y cross-flight direction, z vertical direction), and $\boldsymbol{\sigma}(x,t)$ is the positive definite symmetric concentration-covariance matrix with matrix diagonal elements σ_{yy} and σ_{zz}, and diagonal elements $\sigma_{yz}= \sigma_{zy}$. $A = \iint \exp[-(1/2)\mathbf{x}^T\boldsymbol{\sigma}^{-1}\mathbf{x}]dy\, dz = 2\pi\, [\det(\boldsymbol{\sigma})]^{1/2}$. The initial plume has an elliptical cross-section with effective width B and depth D, $\sigma_{yy} = B^2/8$, $\sigma_{zz}=D^2/8$, so that the initial cross-section area is $A = (\pi/4)\, B\, D$.

The model distinguishes 3 model phases: Phase 0: initial plume conditions just after engine exit; phase 1: initial plume conditions at the end of the wake vortex period (accounting for wake vortex downwash); Phase 2: plume evolution until dry-out because of ambient subsaturation or until sedimentation of the particles below the lower boundary of the computational domain (typically at 5 km altitude).

In phase 0, contrails form when the Schmidt-Appleman criterion is satisfied, i.e. when the ambient temperature T is below a critical temperature T_{LC} (Schumann, 1996) which is a function of fuel properties and the overall propulsion efficiency $\eta = (V\, F)/(m_F\, Q)$, with thrust F, true air speed V, fuel consumption per unit distance m_F and combustion heat Q, and ambient temperature T, absolute ambient humidity q, and pressure p as computed for the given time t and position $\mathbf{x}$ by bilinear interpolation in the NWP output fields. Contrails are assumed to persist when the relative humidity over ice (RHi) is larger than a critical value RHi_{crit}, which should be 100 % for good NWP input data. The ECMWF model output predicts supersaturated air masses fairly realistically (Tompkins et al., 2007). The COSMO-DE model output shows practically no supersaturation. Therefore, we run the model for this example with both input data with $RHi_{crit} = 0.9$.

The initial contrail depth is assumed to be proportional to the wake vortex maximum downwash Δz_w. This downwash is determined from a parameterization of P2P model results (Holzäpfel, 2006). The parameterization is a function of aircraft parameters (mass, speed, span width) and atmospheric parameters (Brunt Vaisaila frequency, density, and turbulent dissipation rate). The aircraft parameter values are taken from the BADA data set of EUROCONTROL.

For microphysics, we assume saturation inside the contrail plume. The initial ice water content IWC in the plume at stage 0 is set to the amount of water mass per volume in the ambient air above ice saturation. The specific water mass in the plume is the sum of ambient humidity and the amount of water emitted from the engine and mixed over the plume cross-section. During the wake vortex phase, the plume sinks and heats up adiabatically. This leads to a reduction of the saturation water mass and hence to a loss of IWC, which is computed within CoCiP accordingly.

The initial number of ice particles N per unit length is assumed to be determined by fuel consumption m_F and the soot number emission index EI_{soot}; this is consistent with recent model results (Kärcher and Yu, 2009) and the few available measurements (Schumann et al., 2002). The soot emission index is estimated according to earlier studies (Petzold et al., 1999; Eyers et al., 2005). During the wake vortex period, part of the ice particles sublimate because of the adiabatic warming and turbulent mixing with ambient air (Sussmann and Gierens, 1999). Loss factors have been computed by large eddy simulations (Kärcher et al., 2009). However, from comparisons to observed data, we got the impression that these factors are too low. Therefore we instead assume that the ratio of N in phase 1 relative to N in phase 0 is proportional to corresponding ratio of IWC.

In the evolution phase (2) of the contrails we follow the plumes in a Lagrangian manner. The plume position follows horizontal and vertical wind as analysed from the NWP data. In addition, the vertical position changes with the mean sedimentation speed of the bulk of the ice particles. We also have foreseen a rising motion component due to radiative heating. For given winds from NWP, advection is computed using a second-order Runge-Kutta scheme.

The change in plume cross-section with time as a function of vertical velocity shear S, and vertical and horizontal diffusivities D_{yy} and D_{zz} is integrated analytically (Konopka, 1995). The diffusivities are functions of plume scales, total shear S_T and stratification N_{BV} (D_{zz}= 0.4 w^2/N_{BV}; w=0.1 m/s as the vertical turbulent velocity fluctuations), $D_{yy} = 0.1\ D^2\ S_T$. The shear diffusivity D_{yz} is set to zero. The shear value S (perpendicular to the plume axis) and S_T (total) are computed from differences of the corresponding wind speeds at the next available levels above and below the contrail. Since the grid spacing Δz is often large compared to the contrail depth D, we allow for an enhancement factor $f(\Delta z/D)$ (Adelfang, 1971), where $f(r) = (1/2)(1+r^m)$. The exponent m is close to 2/3 for Kolmogorov type turbulence (dependence on wavenumber k as $k^{-5/3}$) and close to 0 for 2d turbulence (k^{-3}). Here, we assume m= ½. We also have foreseen enhanced turbulent diffusivities due to radiative heating.

During integration we assume that any ice supersaturation within the air mass entrained with growing cross-section A(t) into the contrail plume gets converted to ice water content $IWC_s(t)$ immediately, leaving saturated ($RHi = RHi_{crit}$) humidity inside the contrail. Accordingly, we integrate the ice water content such that the plume ice water budget is conserved except for mixing with the humidity from ambient air. The volume mean ice particle radius r is computed locally from IWC and number N of ice particles per unit length, or n per unit volume n= N/A, so that $(4/3)\ \pi\ r^3\ n\ \rho_{ice}$ = IWC (ρ_{ice} = 917 kg/m^3 as ice bulk density). We assume that the number of ice particles remains constant unless specific particle loss processes like agglomeration or turbulent phase changes reduce the number of particles. Hence the number of ice particles follows from $dN/dt = (dN/dt)_{agg} + (dN/dt)_{turb}$. Further we use the assumptions $(dN/dt)_{agg} = -E_a\ 8\ \pi\ r^2\ V_t\ N^2/A$, and $(dN/dt)_{turb} = -E_T\ (D_{yy}/\max(D,B)^2 + D_{zz}/d_{eff}^2)\ N$, where V_t is the sedimentation velocity of particles with radius r, and d_{eff} = A/B, and E_a and E_T are free model parameters of order unity. These relationships are justified by dimensional analysis.

The solar optical depth τ of the contrail is computed from $\tau = 3\ Q_{ext}\ IWC\ d_{eff}/(4\ \rho_{ice}\ r_{eff})$, with extinction coefficient Q_{ext}=2 and optically effective radius $r_{eff} = C_\tau\ r$. The factor $C_\tau \cong 0.9$ depends on the particle habits and the particle size distribution function; its value is quite uncertain. The values of τ and r_{eff} form the input to a radiative forcing (RF) model which computes the RF from contrails for given OLR and RSR at TOA fit to forward calculations with libRadtran (Schumann et al., 2009).

3 APPLICATION EXAMPLES

The model has been applied to weather and traffic conditions over Germany and the North Atlantic (first global tests have also been performed) for the following case studies: 1) comparison to insitu measurements of NO_x, ice and soot particle concentrations in the contrails of six (small and large) different aircraft, at plume ages of 60 to 600 s, during the experiment CONCERT, Nov 19, 2008 (Voigt et al., 2009); 2) comparison to lidar measurements of the extinction coefficient of cirrus and contrail cirrus particles at altitudes 6-11 km along a flight path of the Falcon over Germany on Oct 18, 2008 (Schumann and Wirth, 2009); and 3) comparisons to cirrus cover and outgoing longwave radiation data obtained from Meteosat for Germany (see Fig 1) or the North Atlantic in the time period August 11-14 2005. The results show: CoCiP computes a dilution with time which agrees favourable with the NO_x measurements (Voigt et al., 2009) and with previous data (Schumann et al., 1998). The number of ice particles and soot particles computed by CoCiP compares reasonably with insitu measurements during CONCERT. The results do fit only after taking the specific aircraft properties into account. There are no indications of additional ice formation after the initial soot-controlled contrail formation. The diurnal cycle of cirrus cover and OLR computed for 3 days in the NAR shows the order of magnitude with respect to the amplitudes of cirrus cover and of OLR as derived from Meteosat (Graf et al., 2009). Also the delay time between traffic maximum and cirrus cover maximum is in the same range of 3 to 5 h as observed. Parameter studies indicate that changes of most model parameters have less than linear impact on integral results like net radiative

forcing. A somewhat larger sensitivity is found for the critical relative humidity, and the parameters limiting the plume life time. The SW RF is strongly sensitive to the assumed particle habits.

For example, Figure 1 shows the 848 contrails (1069 contrail segments) that are computed to exist in the region shown at 15 UTC this day. The contrails formed from 2816 flights during the 6 h before this time. The average contrail age is 2.25 h. About 38 % of all flights (628626 flight km) in that period formed contrails. The mean fuel flow rate of contrail forming aircraft was 3.8 kg/km. The mean contrail width is 3180 m, the mean contrail length 134 km. More than 92 % of the contrails formed inside the thin cirrus, i.e. in air masses containing positive ice water content, according to ECMWF. Contrails contained 5.3×10^{11}/m ice particles per unit plume length. The mean optical depth τ was 0.054. One contrail reached $\tau = 1.1$. Not accounting for overlap of the various contrails, the cover with thin contrail cirrus would be 110 %, mostly optical thin ($\tau<0.03$). The fraction of cirrus with optical depth larger 0.4 (larger 0.05) was 4.5 % (35.5 %) without contrails and 9 % (50.6 %) with contrails, i.e. 15 % of the sky was covered with contrail cirrus of $\tau>0.05$. The contrail induced RF is 3.8 W/m^2 in the LW, -4.5 W/m^2 in the SW, and -0.64 W/m^2 net. Hence, contrails were cooling in this case. The computed contrail cover agrees - not ideally but qualitatively - with the cirrus cover derived from Meteosat (see Fig. 1). The remaining differences are mainly because of deviations of the computed RHi from the NWP data compared to reality. Best performance was obtained with ECMWF forecasts from 12 UTC that day.

4 CONCLUSIONS

A new Contrail Cirrus Prediction Tool (CoCiP) has been developed to simulate and predict contrail cirrus from a fleet of aircraft, flight by flight, regionally or globally. The model has been developed in the last year and parts are still under development. So far, the model has been tested in parameter studies in comparison with insitu, lidar, and satellite data. The most critical parameters concern the NWP humidity and the life time of contrails (sedimentation, turbulent particle loss). The results indicate that most contrails occur inside thin cirrus in the upper troposphere. The radiative forcing by contrail cirrus is far larger than estimated from line shaped contrails and may be negative at least regionally. Contrail climate impact can be reduced by proper air traffic management. The model will next be used for global evaluation of contrail cirrus RF. We plan to run it for several years and compare it with Meteosat observations. Moreover we plan for tests with research aircraft (HALO and Falcon) in a cirrus experiment “ML-CIRRUS”. The model will also be applied within the project UFO (Mannstein and al., 2009). In the future, the model may be coupled to other global models (with aerosols & chemistry) to assess the total aviation climate impact. For example it may be used to study renucleation effects from contrail-processed soot emissions. The model may be extended with plume chemistry to compute the effective chemical emissions. Higher order microphysics cloud physics may be included. The same principle approach may be used to simulate ship trails.

5 ACKNOWLEDGMENTS

The author gratefully acknowledges contributions from coworkers, in particular: K. Graf, B. Mayer, H. Mannstein, U. Hamann, R. Meerkötter (help with Meteosat, MeCiDa, LibRadTran), M. Wirth, S. Rahm (lidar), C. Voigt, T. Jurkat, H. Schlager et al. (CONCERT), F. Holzäpfel (P2P model), A. Dörnbrack, C. Keil, J. Dahl, and A. Tafferner (for access to NWP data), and K. Gierens, I. Sölch, and S. Unterstraßer (modelling). Moreover, important meteorological data and air traffic data were provided by DWD, ECMWF, DFS, and EUROCONTROL. This research is part of the DLR-project “Climate-compatible Air Transport System” (CATS).

REFERENCES

Adelfang, S. I., 1971: On the relations between wind shears over various altitude intervals. *J. Appl. Meteorol.*, *10*, 156-159.

Dürbeck, T. and T. Gerz, 1996: Dispersion of aircraft exhausts in the free atmosphere. *J. Geophys. Res.*, *101*, 26007-26015.

Eyers, C. J., D. Addleton, K. Atkinson, et al., 2005: AERO2k Global Aviation Emissions Inventories for 2002 and 2025.

Graf, K., H. Mannstein, B. Mayer, and U. Schumann, 2009: Aviation fingerprint in diurnal cycle of cirrus over the North Atlantic. *Intern. Conf. on Transport, Atmosphere and Climate*, Aachen and Maastricht, EUR, this volume.

Holzäpfel, F., 2006: Probabilistic Two-Phase Aircraft Wake-Vortex Model: Further Development and Assessment. *J. Aircraft*, *43***,** 700-708.

IPCC, 1999: *Aviation and the Global Atmosphere*. Cambridge Univ. Press, 373 pp.

IPCC, 2007: *Climate Change 2007: The Physical Science Basis. Contribution of Working Group I to the Fourth Assessment Report of the Intergovernmental Panel on Climate Change*. Cambridge Univ. Press, 996 pp.

Kärcher, B., U. Burkhardt, S. Unterstrasser, and P. Minnis, 2009: Factors controlling contrail cirrus optical depth. *Atmos. Chem. Phys.*, *9***,** 6229-6254.

Kärcher, B. and F. Yu, 2009: Role of aircraft soot emissions in contrail formation. *Geophys. Res. Lett.*, *36***,** L01804.

Konopka, P., 1995: Analytical Gaussian solutions for aniosotropic diffusion in a linear shear flow. *J. Non-Equilib. Thermodyn.*, *20***,** 78-91.

Krebs, W., H. Mannstein, L. Bugliaro, and B. Mayer, 2007: Technical note: A new day- and night-time Meteosat Second Generation Cirrus Detection Algorithm MeCiDA. *Atmos. Chem. Phys.*, *7***,** 6145-6159.

Lee, D. S., G. Pitari, V. Grewe, et al., 2009: Transport impacts on atmosphere and climate: Aviation. *Atmos. Env.***,** 1–57.

Mannstein, H. and al., 2009: Smart aircraft routing – a possibility for mitigation? *Intern. Conf. on Transport, Atmosphere and Climate*, Sausen, Ed., EUR.

Petzold, A., A. Döpelheuer, C. A. Brock, and F. Schröder, 1999: In situ observation and model calculations of black carbon emission by aircraft at cruise altitude. *J. Geophys. Res.*, *104***,** 22171-22181.

Schumann, U., 1994: On the effect of emissions from aircraft engines on the state of the atmosphere. *Ann. Geophysicae*, *12***,** 365-384.

Schumann, U., 1996: On conditions for contrail formation from aircraft exhausts. *Meteorol. Z.*, *5***,** 4-23.

Schumann, U., F. Arnold, R. Busen, J. Curtius, B. Kärcher, J. Curtius, A. Petzold, H. Schlager, F. Schröder, and K. H. Wohlfrom, 2002: Influence of fuel sulfur on the composition of aircraft exhaust plumes: The experiments SULFUR 1-7. *J. Geophys. Res.*, *107***,** AAC 2-1 - AAC 2-27.

Schumann, U. and P. Konopka, 1994: A simple estimate of the concentration field in a flight corridor. *Impact of Emissions from Aircraft and Spacecraft upon the Atmosphere. Proc. of an Intern. Sci. Colloquium, Köln (Cologne), Germany, April 18-20, 1994*, Schumann and Wurzel, Eds., DLR-Mitt. 94-06, 354-359.

Schumann, U., P. Konopka, R. Baumann, R. Busen, T. Gerz, H. Schlager, P. Schulte, and H. Volkert, 1995: Estimate of diffusion parameters of aircraft exhaust plumes near the tropopause from nitric oxide and turbulence measurements. *J. Geophys. Res.*, *100***,** 14147-14162.

Schumann, U., B. Mayer, K. Graf, H. Mannstein, and R. Meerkötter, 2009: A parametric radiative forcing model for cirrus and contrail cirrus. *ESA Atmospheric Science Conference, Special Publication SP-676 (6 pages)*, Barcelona, Spain, 7-11 September 2009, 1-6.

Schumann, U., H. Schlager, F. Arnold, R. Baumann, P. Haschberger, and O. Klemm, 1998: Dilution of Aircraft Exhaust Plumes at Cruise Altitudes. *Atmos. Env.*, *32***,** 3097 - 3103.

Schumann, U. and M. Wirth, 2009: Optical depth of cirrus and embedded contrails from airborne Lidar and models *Geophysical Research Abstracts, EGU2009-5128*, *11***,** 1.

Sussmann, R. and K. Gierens, 1999: Lidar and numerical studies on the different evolution of vortex pair and secondary wake in young contrails. *J. Geophys. Res.* , *104***,** 2131-2142.

Tompkins, A., K. Gierens, and G. Rädel, 2007: Ice supersaturation in the ECMWF Integrated Forecast System. *Q. J. R. Meteorol. Soc.*, *133***,** 53–63.

Voigt, C., U. Schumann, T. Jurkat, and al., 2009: Detection of young contrails – selected results from the CONCERT (CONtrail and Cirrus ExpeRimenT) campaign. *Intern. Conf. on Transport, Atmosphere and Climate*, Aachen and Maastricht, EUR, this volume.

A global ship track climatology from ATSR-2: January 1999 – January 2001

A. M. Sayer*, R. G. Grainger
Atmospheric, Oceanic and Planetary Physics, Department of Physics, University of Oxford, UK

E. Campmany
NASA Goddard Institute for Space Studies, New York, USA

Keywords:

ABSTRACT: Two years (January 1999 – January 2001) of data from the Along-Track Scanning Radiometer 2 (ATSR-2) aboard the satellite ERS-2 have been processed with an automatic ship track detection algorithm. The distribution of detected tracks shows similar patterns and magnitudes to another satellite-derived dataset and is consistent with locations of shipping lanes. Most tracks are detected in the North Pacific and North Atlantic, between March and August. The derived track masks have been used with ATSR-2 data from the Oxford-RAL Aerosol and Clouds (ORAC) retrieval scheme to reveal differences between track and non-track clouds. Water clouds which are part of a ship track show an approximate 50% increase in optical depth as compared to background cloud conditions (30 km or more from tracks), and a decrease in effective radius of similar magnitude. This is consistent with the first aerosol indirect (Twomey) effect.

1 INTRODUCTION

The aerosol present in the exhaust of ships can act as cloud condensation nuclei (CCN) and seed clouds in clear-sky situations, or alternatively the increase in CCN can modify the properties of existing clouds. Such resulting ship tracks are easily visible in aerial or satellite imagery, although their global spatial extent and impact on cloud properties are less well-known. Hence it is of interest to be able to quantify them.

In this work the application of an algorithm for the automatic detection of ship tracks from near-infrared Along-Track Scanning Radiometer 2 (ATSR-2) imagery, combined with retrievals of cloud microphysical properties derived from the same instrument, is discussed. The ATSR-2 instrument was launched in 1995 on the satellite ERS-2 and measures radiance at 7 wavelengths in the visible and infrared; nadir-view measurements from the 0.67, 0.87, 1.6, 10.8 and 12.0 μm channels are used in the track detection and cloud retrieval algorithms. At present, data from January 1999 to January 2001 have been processed with the ship track detection algorithm.

2 TRACK DETECTION AND FILTERING

The automated ship-track detection algorithm is described in detail by Campmany et al., (2009). It uses ATSR-2 1.6 μm data gridded to 3 km by 4 km pixels to find straight 'ridgelets' of higher intensity than their neighbours. These ridgelets are then connected via a set of connectivity rules, and are deemed to be ship tracks if sufficiently long. Additional constraints, such as the absolute 1.6 μm intensity of the pixels and their infrared brightness temperatures, are employed to ensure that the detected ridgelets represent low-lying cloud.

Detected tracks are then filtered using data from the Oxford-RAL Aerosol and Clouds (ORAC) retrieval scheme, processed under the framework of the Global Retrieval of ATSR Cloud Parameters and Evaluation (GRAPE) project (Poulsen et al., in prep., Sayer et al., in prep.). The ORAC data provides (with associated uncertainty estimates and quality control information) for each

* *Corresponding author:* Andrew Sayer, University of Oxford – Clarendon Laboratory, Parks Road, Oxford, OX1 3PU. Email: sayer@atm.ox.ac.uk

cloudy pixel estimates of the cloud optical depth, effective radius, water path, and cloud-top pressure (also converted to height and temperature), along with information on whether the cloud consists of water droplets or ice crystals. The track detection is performed at 3 km by 4 km resolution as the retrieval of cloud properties is performed at this scale. The ORAC algorithm has been applied to the whole ATSR-2 dataset and is currently being applied to the similar Advanced ATSR (AATSR) instrument, launched in 2002 as the successor instrument to ATSR-2.

Pixels flagged as potential tracks by the automatic algorithm are then confirmed as track pixels if they correspond to successful water cloud retrievals with a cloud-top height lower than 1 km. This extra step helps to remove false positives from the detections.

3 DISTRIBUTION OF DETECTED TRACKS

The annual mean fractional coverage of ship tracks is shown in Figure 1. Tracks are most frequently detected in the Northern Atlantic and Pacific oceans, where annual mean coverage may reach 0.3 % in some regions. This distribution of tracks is consistent with known heavy shipping traffic in these regions (Endrensen et al., 2003) although shipping lanes elsewhere in the world without track detections are a consequence of the meteorology, with track formation requiring low warm, moist air. The distribution is also consistent with the results of Schreier et al., (2007) who detected ship tracks in AATSR data for the year 2004.

Track frequency was found to exhibit a seasonal cycle, with more tracks detected in the Summer hemisphere (particularly in the Northern Hemisphere between March and August). This is again consistent with Schreier et al., (2007); as shipping traffic does not show this seasonal behaviour, this is further evidence for the meteorological dependence of ship track occurrence.

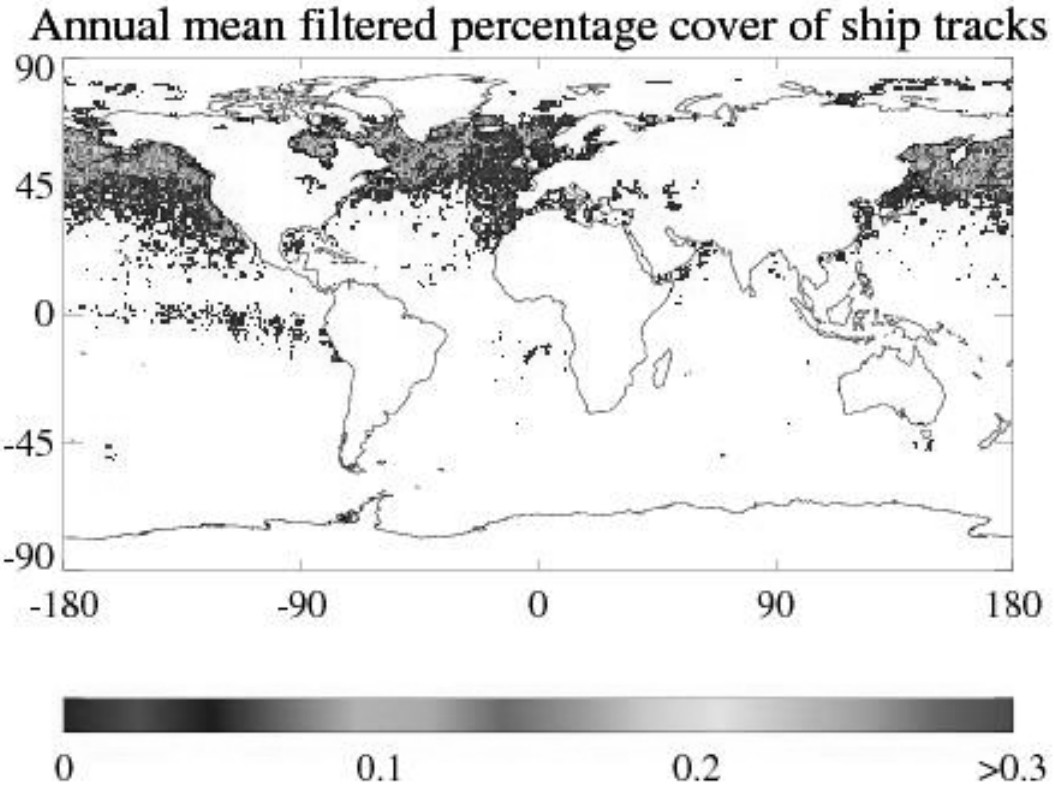

Figure 1. Annual mean percentage cover of ship tracks determined for the period January 1999-January 2001, after the automated detection algorithm and ORAC cloud retrieval filter have been applied.

4 PROPERTIES OF TRACK AND NEAR-TRACK CLOUDS

Together with the track mask, the ORAC cloud retrieval data enable the comparison of ship track properties with those of nearby cloud. This allows the assessment of the impact of shipping on ex-

isting cloud decks (although does not directly inform about the properties of new clouds seeded in otherwise cloud-free conditions).

For each orbit containing ship tracks, the mean cloud optical depth, effective radius, and liquid water path are calculated for retrievals flagged as being parts of tracks. Then, the same calculation is done for water cloud retrievals at increasing distances from the nearest pixel flagged as a track, in 4 km distance increments (e.g. 0-4 km, 4-8 km). Finally the ratio between the mean cloud property for track pixels and that for cloud properties for each distance increment are found. As ship tracks tend to be geographically clustered and so subject to similar background meteorological conditions, calculating these means on an orbit basis, rather than the more difficult task of by individual tracks, is not expected to influence the comparison.

This process is repeated for each orbit containing tracks to form a mean distance profile; Figure 2 shows the relative cloud optical depth moving away from tracks, Figure 3 the relative cloud effective radius, and Figure 4 the relative cloud water path. These figures show that the tracks have a higher cloud optical depth and lower effective radius than background conditions (where the background, taken at the point at which the curves flatten, is approximately 30 km from the nearest track pixel). The tracks show an enhancement of the order of 50 % in optical depth and decrease of a similar amount (although not quite as pronounced) in effective radius as compared to these background values. This result is consistent with the first aerosol indirect effect (also called the Twomey effect or cloud albedo effect) that the aerosol from the ship's exhaust leads to a higher number of smaller cloud droplets.

The liquid water path, shown in Figure 4, is approximately constant but shows a hint of enhancement near tracks. Liquid water path is calculated from the product of optical depth and effective radius and this enhancement is an indicator of the stronger response of cloud optical depth than effective radius. It is not clear whether the enhancement is real, which could be due to increased water content from convective rising of air in the ship's path, or a retrieval artefact.

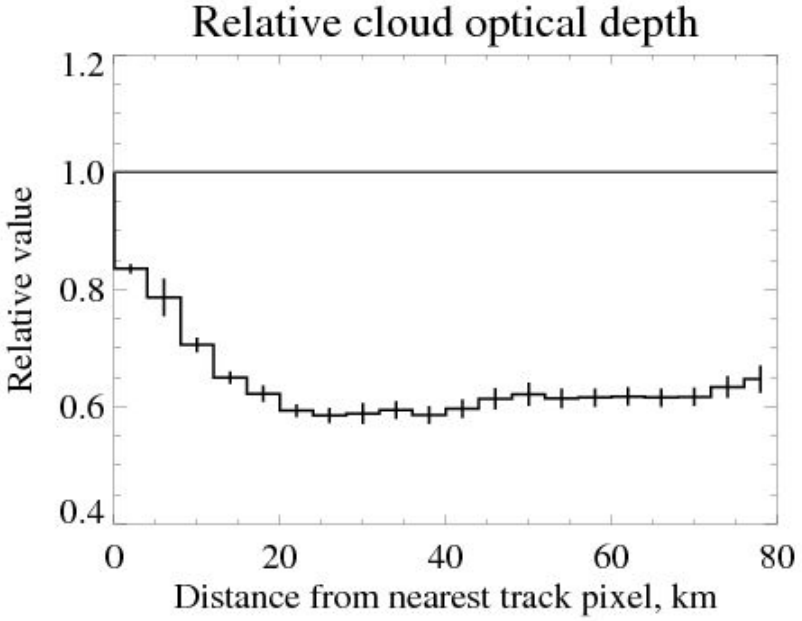

Figure 2. Relative cloud optical depth as a function of distance from nearest track pixel. The error bars indicate the standard error on each distance increment. The solid grey line indicates a ratio of 1.

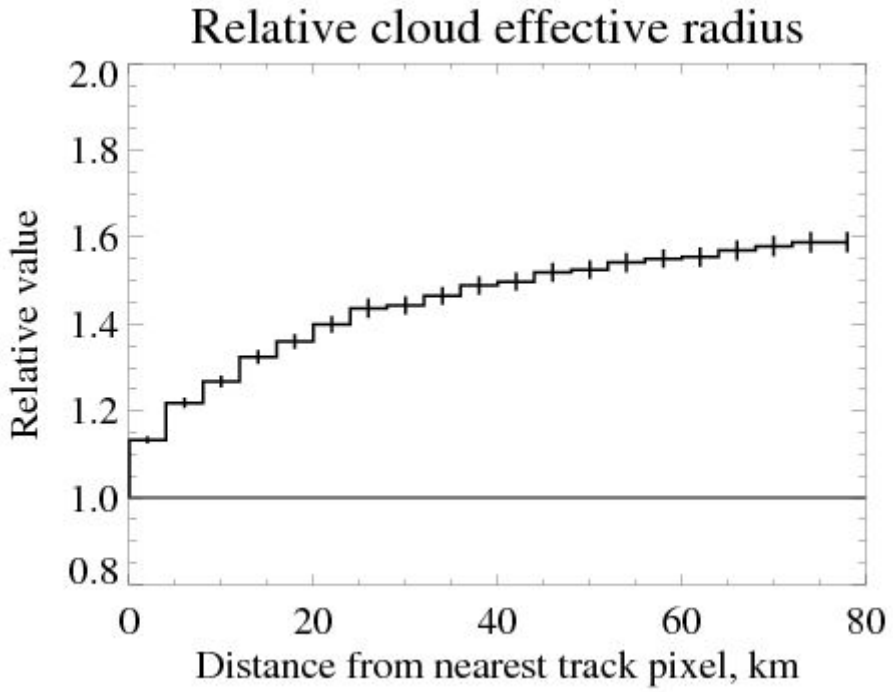

Figure 3. Relative cloud effective radius as a function of distance from nearest track pixel. The error bars indicate the standard error on each distance increment. The solid grey line indicates a ratio of 1.

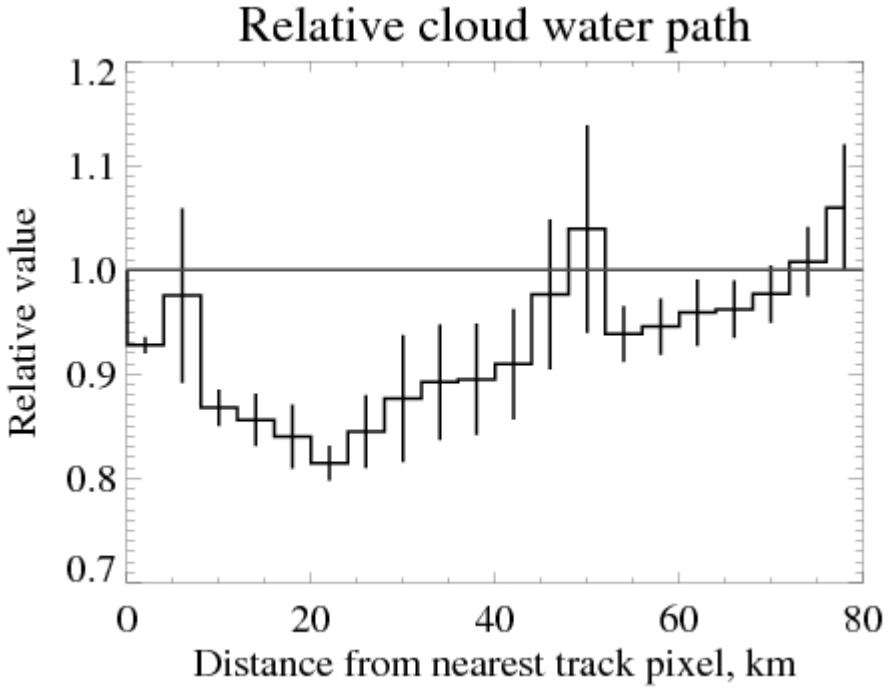

Figure 4. Relative cloud liquid water path as a function of distance from nearest track pixel. The error bars indicate the standard error on each distance increment. The solid grey line indicates a ratio of 1.

5 CONCLUSIONS

An automatic algorithm for the detection of ship tracks has been applied to two years of data from ATSR-2. The distribution of detected tracks is consistent with known patterns of shipping, and another satellite dataset of ship track frequency.

The change of cloud optical depth, effective radius and liquid water path has been examined as a function of distance from ship tracks. This revealed an approximate 50 % increased of optical depth

and a decrease of effective radius of slightly smaller magnitude as compared to background conditions 30 km or more away. This is a signature of the first aerosol indirect effect on clouds. Liquid water path showed signs of a small enhancement in and near tracks although the reasons for this are not certain.

Although at an early stage, this work demonstrates the capability to monitor ship track occurrence and properties from space. In the future this algorithm will be improved and applied to the whole (A)ATSR record to give a 13-year or longer record of ship tracks, which could be used to further investigate aerosol indirect effects, examine trends in shipping and ship-induced cloudiness and estimate the radiative forcing of ship tracks.

REFERENCES

Campmany, E., R. G. Grainger, S. M. Dean, and A. M. Sayer, 2009: Automatic detection of ship tracks in ATSR-2 satellite imagery. *Atmos. Chem. Phys., 9*, 1899-1905.

Endresen, O., E. Sørgard, J. K. Sundet, S. B. Dalsøren, I. S. Isaksen, T. F. Berglen, and G. Gravir, 2003. Emission from international sea transportation and environmental impact. *J. Geophys. Res., 108*, D17.

Poulsen, C. A., E. Campmany, R. G. Grainger, A. M. Sayer, R. Siddans, and G. E. Thomas, in prep. The GRAPE cloud retrieval algorithm.

Sayer, A. M., E. Campmany, R. G. Grainger, C. A. Poulsen, R. Siddans, and G. E. Thomas, in prep. Validation of GRAPE cloud products.

Schreier, M., H. Mannstein, V. Eyring, and H. Bovensmann, 2007. Global ship track distribution and radiative forcing from 1 year of AATSR data. *Geophys. Res. Lett, 34*, L17814.